

# Exploring the Potential of *N*-Benzylidenebenzohydrazide Derivatives as Antidiabetic and Antioxidant Agents: Design, Synthesis, Spectroscopic, Crystal Structure, DFT and Molecular Docking Study

Ibrahim Waziri,<sup>\*[a]</sup> Tunde L. Yusuf,<sup>[b]</sup> Monsuru T. Kelani,<sup>[a]</sup> Eric O. Akintemi,<sup>[c]</sup> Kolawole A. Olofinson,<sup>[d]</sup> and Alfred J. Muller<sup>[a]</sup>

Hydrazone-type Schiff bases have been widely explored owing to their therapeutic properties. These compounds are known to have antibacterial, antifungal, anticancer, and antioxidant properties, among others. In the present study, six hydrazone-based Schiff bases (**BB1**–**BB6**) were synthesized by the reaction between derivatives of benzaldehyde and benzo hydrazide in methanolic medium in the presence of catalytic amount of formic acid. The synthesized compounds were characterized using various spectroscopic techniques such as NMR (<sup>1</sup>H, <sup>13</sup>C, COSY, DEPT, HSQC, HMBC, and NOESY), FTIR, UV-Vis, elemental

(CHN) analysis, and high-resolution mass spectroscopy. In addition, single crystal structures of **BB2**, **BB4**, and **BB6** were obtained. *In vitro* antidiabetic and antioxidant potential of the compounds was evaluated on glucosidase, amylase, NO, FRAP, and DPPH assays, respectively. In all the assays, compounds **BB6**, **BB4**, and **BB2** showed higher activity than the others. To further explore the chemical reactivity properties and their mechanism of action against the tested assays, DFT and molecular docking study were performed, and the results obtained reinforce the experimental study data.

## 1. Introduction

Existence of uncontrolled reactive oxygen species (ROS), such as superoxide radicals, hydroxyl radicals, hydrogen peroxide radicals, or oxidative stress, is detrimental to biological systems.<sup>[1,2]</sup> Several antioxidant enzymatic systems, including superoxide dismutase (SOD), catalase (CAT), glutathione (GSH), and glutathione S-transferase (GST), support the body's natural homeostatic regulation of ROS production and removal.<sup>[3,4]</sup> Disruption of these species can have consequences for various biomolecules, including proteins, carbohydrates, nucleic acids, lipids, and DNA, and may lead to neurodegenerative diseases.<sup>[5]</sup>

Moreover, oxidative stress or inflammation plays a role in disorders such as diabetes and neurodegenerative diseases.<sup>[6–8]</sup> Antioxidants act as shields in these circumstances, preventing biomolecule oxidation and fortifying the immune system against the harmful effects of ROS.<sup>[9–11]</sup> Consequently, researchers are increasingly focusing on designing and discovering synthetic and natural products that can simultaneously serve as antioxidants and antidiabetic agents.<sup>[12,13]</sup> Numerous compounds with dual therapeutic properties have been reported, with Schiff bases being one example.

Schiff base compounds have gained recognition in the field of medicinal chemistry due to the extensive biological properties associated with the azomethine moiety. This class of compounds has been instrumental in the development and design of various lead compounds with medicinal importance.<sup>[14–16]</sup> Additionally, hydrazone-type Schiff bases have exhibited superior activity compared to conventional Schiff bases, particularly aroyl-hydrazones.<sup>[17–19]</sup> These compounds possess adaptable and versatile structural qualities, along with potent pharmacological properties such as anticonvulsant, antidepressant, antimicrobial, antiviral, and antitumor effects.<sup>[20–22]</sup> Aromatic Hydrazone Schiff derivative compounds have garnered significant attention due to their promising antioxidant properties. These compounds possess a unique molecular structure that combines the antioxidant potential of both aromatic hydrazine and Schiff base moieties. Several studies have demonstrated their ability to scavenge free radicals and protect against oxidative stress-related damage. For instance, Ali and colleagues investigated the superoxide dismutase (SOD) mimetic activity of binuclear metal complexes derived from aromatic-hydrazone Schiff bases. The results showed promising activity for both the ligands and their metal

[a] Dr. I. Waziri, M. T. Kelani, Prof. A. J. Muller  
Research Centre for Synthesis and Catalysis, Department of Chemical Sciences, University of Johannesburg, P.O. Box 524, Auckland Park, Johannesburg 2006, South Africa  
E-mail: triumph2236@gmail.com

[b] Dr. T. L. Yusuf  
Department of Chemistry, Faculty of Natural Science and Agricultural Science, University of Pretoria, Private Bag X20, Hatfield 0028 Pretoria, South Africa

[c] Dr. E. O. Akintemi  
Department of Chemistry, University of South Africa, Florida Science Campus, Johannesburg 1709, South Africa

[d] Dr. K. A. Olofinson  
Department of Biochemistry, Faculty of Natural and Applied Sciences, Nile University of Nigeria, Nigeria

Supporting information for this article is available on the WWW under <https://doi.org/10.1002/slct.202401631>

© 2024 The Authors. ChemistrySelect published by Wiley-VCH GmbH. This is an open access article under the terms of the Creative Commons Attribution Non-Commercial NoDerivs License, which permits use and distribution in any medium, provided the original work is properly cited, the use is non-commercial and no modifications or adaptations are made.

complexes, with an  $IC_{50}$  value as low as  $2.5 \pm 0.6 \mu\text{M}$ .<sup>[23]</sup> Similarly, aromatic-hydrazone Schiff bases have been reported to exhibit enhanced radical scavenging activity, inhibiting lipid peroxidation and enhancing endogenous antioxidant defenses, such as superoxide dismutase and glutathione peroxidase activities.<sup>[24,25]</sup> These compounds have also shown antimicrobial and antifungal properties.<sup>[26,27]</sup> Furthermore, hydrazones and their derivatives have demonstrated chemotherapeutic efficacy in the treatment of tuberculosis.<sup>[28,29]</sup> In the context of diabetes, hydrazones and their metal complexes have been investigated for their ability to inhibit enzymes involved in carbohydrate metabolism, such as  $\alpha$ -glucosidase and aldose reductase, which can help regulate blood glucose levels and prevent associated complications.<sup>[30]</sup> Hydrazones possess antioxidant properties due to their ability to scavenge free radicals and inhibit oxidative stress, which is implicated in various diseases, including diabetes. One study conducted by Aslanhan et al. investigated the antioxidant activity of several hydrazones derived from isonicotinic acid hydrazide. The compounds exhibited significant radical-scavenging activity, highlighting their potential as antioxidants.<sup>[31]</sup> These findings emphasize the potential of aromatic Hydrazone Schiff derivatives as effective antioxidants. Some biologically active hydrazone compounds reported in the literature are presented in Table.

Motivated by the fascinating biological properties of aromatic hydrazones and our objective of identifying multi-target agent compounds, this study focuses on the synthesis of six aromatic-hydrazone Schiff bases (BB1–BB6). However, BB1, has previously reported alongside its corrosion inhibition activity.<sup>[37]</sup> We aim to investigate how substituents influence the antioxidant and anti-diabetic activity of these compounds. To gain insights into their electronic characteristics and mode of action, we conducted DFT and molecular docking studies. It is well-known that molecules containing halogens or electron-depleting groups exhibit viable biological properties. The incorporation of these groups has been shown to increase lipophilicity, enhance biological activity, and improve lipid membrane penetration. In our pursuit of enhancing the potential therapeutic and targeted effects of these compounds, we strategically modified their pharmacological properties by incorporating substituents composed of halogen, electron-donating, and electron-withdrawing groups. By doing so, we aim to optimize the compounds' efficacy and explore their potential in diverse therapeutic applications.

## Experimental

### Reagents and Instruments

All the chemicals and reagents used in this research were purchased from Merck Life Sciences (Pty) Ltd and utilized as received without any prior purification. These included benzohydrazide, benzaldehyde, 4-nitrobenzaldehyde, 4-chlorobenzaldehyde, and p-toluic hydrazide.

For the characterization and structural elucidation of the synthesized compounds, various spectroscopic techniques were employed. These techniques included  $^1\text{H}$  and  $^{13}\text{C}$  NMR spectroscopy,

Fourier-transform infrared spectroscopy (FTIR), UV-Vis spectroscopy, single crystal X-ray diffraction, mass spectroscopy, and CHN elemental analysis.

### General Procedure for the Synthesis of the Compounds

To synthesize the compounds, a modified version of a simple condensation reaction procedure reported in the literature<sup>[14,15,38]</sup> was adopted. In general, a solution of the benzohydrazide derivatives (1 mmol, 1 eq) in 20 mL of methanol each in a separate reaction flask was reacted with the solution of the benzaldehyde derivatives (1 mmol, 1 eq) in 20 mL of methanol each in a separate reaction flask, and catalytic amount of formic acid (three drops) was added to the mixture and stirred at room temperature for 3 hrs. The resulting precipitate was filtered and washed with methanol to remove any unreacted components. Subsequently, the precipitate was washed with ether and allowed to dry. The reaction scheme is depicted below. For the compounds **BB2**, **BB4**, and **BB6**, single crystals suitable for single crystal X-ray diffraction analysis were obtained after three days by dissolving approximately 2–3 mg of the dried product in hot methanol and allowing it to crystallize through slow evaporation.

### N-Benzylidenebenzohydrazide BB1

White powder; M.p.: 180–183 °C; yield: 1.2 g (80%);  $IR_{\text{ATR}}$  ( $\nu_{\text{max}}/\text{cm}^{-1}$ ): 3200 (NH), 2800 (C–H), 1720 (C=O), 1610 (C=N); UV-Vis (DMSO,  $10^{-3}$  M, nm): 264 ( $\pi \rightarrow \pi^*$ ), 298 ( $n \rightarrow \pi^*$ );  $^1\text{H}$  NMR (DMSO- $d_6$ , 500 MHz,  $\delta$  ppm) 11.88 (s, 1H, NH), 8.49 (s, 1H, HC=N), 7.94 (d, 2H,  $J=7.5$  Hz, Aromatic-H), 7.74 (d, 2H,  $J=6.0$  Hz, Aromatic-H), 7.59 (d, 1H,  $J=6.5$  Hz, Aromatic-H), 7.54 (t, 2H,  $J=7.5$  Hz, Aromatic-H), 7.46 (d, 3H,  $J=7.0$  Hz, Aromatic-H);  $^{13}\text{C}$  NMR (DMSO- $d_6$ , 126 MHz,  $\delta$  ppm) 163.11 (1 C, C=O), 147.79 (1 C, C=N), 134.31, 133.42, 131.64, 129.98, 128.76, 128.39, 127.55, 127.02 (Aromatic-C); Anal. Calcd. (%) for  $\text{C}_{14}\text{H}_{12}\text{N}_2\text{O}$  (224.0950): C, 74.98; N, 12.49; H, 5.39; Found: C, 74.34; N, 12.44; H, 5.57; MS ( $m/z$ ): Calcd. = 225.1028  $[\text{M} + \text{H}]^+$ ; Found = 225.1025  $[\text{M} + \text{H}]^+$ .

### N-(4-Nitrobenzylidene)Benzohydrazide BB2

Off white powder; M.p.: 200–203 °C; yield: 1.27 g (82%);  $IR_{\text{ATR}}$  ( $\nu_{\text{max}}/\text{cm}^{-1}$ ): 2700 (C–H), 3100 (NH), 1718 (C=O), 1605 (C=N), 1500 ( $\text{NO}_2$ ), 1270 ( $\text{NO}_2$ ); UV-Vis (DMSO,  $10^{-3}$  M, nm): 266 ( $\pi \rightarrow \pi^*$ ), 347 ( $n \rightarrow \pi^*$ );  $^1\text{H}$  NMR (DMSO- $d_6$ , 500 MHz,  $\delta$  ppm): 12.15 (s, 1H, NH), 8.54 (s, 1H, HC=N), 8.29 (d, 2H,  $J=8.0$  Hz, Aromatic-H), 7.99 (d, 2H,  $J=7.5$  Hz, Aromatic-H), 7.93 (d, 2H,  $J=6.5$  Hz, Aromatic-H), 7.60 (d, 1H,  $J=6.5$  Hz, Aromatic-H), 7.55 (t, 2H,  $J=7.5$  Hz, Aromatic-H);  $^{13}\text{C}$  NMR (DMSO- $d_6$ , 126 MHz): 163.36 (1 C, C=O) 147.81 (1 C, C=N), 145.21, 140.62, 133.06, 131.94, 128.45, 127.92, 127.68, 123.99 (Aromatic-C); Anal. Calcd. (%) for  $\text{C}_{14}\text{H}_{11}\text{N}_3\text{O}_3$  (269.0800): C, 62.45; N, 15.61; H, 4.12; Found: C, 62.58; N, 15.68; H, 4.12; MS ( $m/z$ ): Calcd. = 270.0879  $[\text{M} + \text{H}]^+$ ; Found = 270.0889  $[\text{M} + \text{H}]^+$ .

### N-Benzylidene-4-Methylbenzohydrazide BB3

White powder; M.p.: 236–240 °C; yield: 1.34 g (88%);  $IR_{\text{ATR}}$  ( $\nu_{\text{max}}/\text{cm}^{-1}$ ): 2800 (C–H), 3200 (NH), 1700 (C=O), 1600 (C=N); UV-Vis (DMSO,  $10^{-3}$  M, nm): 268 ( $\pi \rightarrow \pi^*$ ), 306 ( $n \rightarrow \pi^*$ );  $^1\text{H}$  NMR (DMSO- $d_6$ , 500 MHz,  $\delta$  ppm): 11.77 (s, 1H, NH), 8.48 (s, 1H, HC=N), 7.84 (d, 2H,  $J=6.5$  Hz, Aromatic-H), 7.73 (s, 2H, Aromatic-H), 7.45 (d, 3H,  $J=7.0$  Hz, Aromatic-H), 7.33 (d, 2H,  $J=7.5$  Hz, Aromatic-H), 2.37 (s, 3H,  $\text{CH}_3$ );  $^{13}\text{C}$  NMR (DMSO- $d_6$ , 126 MHz,  $\delta$  ppm): 162.99 (1 C, C=O) 147.56 (1 C, C=N) 141.77, 134.39, 130.53, 129.96, 128.96, 128.79, 127.60, 127.01 (Aromatic-C), 20.98 (1 C,  $\text{CH}_3$ ); Anal. Calcd. (%) for  $\text{C}_{15}\text{H}_{14}\text{N}_2\text{O}$

(238.1106): C, 75.61; N, 11.76; H, 5.92; Found: C, 75.68; N, 11.81; H, 5.93; MS (*m/z*): Calcd. = 239.1184 [M + H]<sup>+</sup>; Found = 239.1207 [M + H]<sup>+</sup>.

#### 4-Mmethyl-N-(4-Nitrobenzylidene)Benzohydrazide BB4

Grey powder; M.p.: 220–223 °C; yield: 1.18 g (85%); IR<sub>ATR</sub> ( $\nu_{max}/\text{cm}^{-1}$ ): 2750 (C–H), 3150 (NH), 1700 (C=O), 1595 (C=N), 1500 (NO<sub>2</sub>), 1280 (NO<sub>2</sub>); UV-Vis (DMSO, 10<sup>-3</sup> M, nm): 266 ( $\pi \rightarrow \pi^*$ ), 349 ( $n \rightarrow \pi^*$ ); <sup>1</sup>H NMR (DMSO-*d*<sub>6</sub>, 500 MHz,  $\delta$  ppm): 12.07 (s, 1H, NH), 8.53 (s, 1H, HC=N), 8.29 (d, 2H, *J* = 8.0 Hz, Aromatic-H), 7.98 (d, 2H, *J* = 7.0 Hz, Aromatic-H), 7.84 (d, 2H, *J* = 6.5 Hz, Aromatic-H), 7.34 (d, 2H, *J* = 8.0 Hz, Aromatic-H), 2.38 (s, 3H, CH<sub>3</sub>); <sup>13</sup>C NMR (DMSO-*d*<sub>6</sub>, 126 MHz,  $\delta$  ppm): 163.21 (1 C, C=O), 147.78 (1 C, C=N), 144.95, 142.12, 140.71, 130.17, 129.01, 127.90, 127.73, 124.02 (Aromatic-C), 21.01 (1 C, CH<sub>3</sub>); Anal. Calcd. (%) for C<sub>15</sub>H<sub>13</sub>N<sub>3</sub>O<sub>3</sub> (283.0957): C, 63.60; N, 14.83; H, 4.63; Found: C, 63.89; N, 14.87; H, 4.78; MS (*m/z*): Calcd. = 284.1035 [M + H]<sup>+</sup>; Found = 284.1064 [M + H]<sup>+</sup>.

#### N-(4-Chlorobenzylidene)-4-Methylbenzohydrazide BB5

Grey powder; M.p.: 210–213 °C; yield: 1.31 g (82%); IR<sub>ATR</sub> ( $\nu_{max}/\text{cm}^{-1}$ ): 2900 (C–H), 3200 (NH), 1705 (C=O), 1610 (C=N); UV-Vis (DMSO, 10<sup>-3</sup> M, nm): 275 ( $\pi \rightarrow \pi^*$ ), 319 ( $n \rightarrow \pi^*$ ); <sup>1</sup>H NMR (DMSO-*d*<sub>6</sub>, 500 MHz,  $\delta$  ppm): 11.86 (s, 1H, NH), 8.44 (s, 1H, HC=N), 7.83 (d, 2H, *J* = 7.5 Hz, Aromatic-H), 7.75 (d, 2H, *J* = 8.0 Hz, Aromatic-H), 7.51 (d, 2H, *J* = 8.0 Hz, Aromatic-H), 7.33 (d, 2H, *J* = 7.5 Hz, Aromatic-H), 2.37 (s, 3H, CH<sub>3</sub>); <sup>13</sup>C NMR (DMSO-*d*<sub>6</sub>, 126 MHz,  $\delta$  ppm): 162.95 (1 C, C=O), 146.12 (1 C, C=N), 141.80, 134.38, 133.33, 130.42, 128.93, 128.86, 128.59, 127.60 (Aromatic-C), 20.97 (1 C, CH<sub>3</sub>); Anal. Calcd. (%) for C<sub>15</sub>H<sub>13</sub>ClN<sub>2</sub>O (272.0716): C, 66.06; N, 10.27; H, 4.80; Found: C, 65.90; N, 10.49; H, 4.76; MS (*m/z*): Calcd. = 273.0795 [M + H]<sup>+</sup>; Found = 273.0817 [M + H]<sup>+</sup>.

#### N-(4-Chlorobenzylidene)Benzohydrazide BB6

White crystal; M.p.: 177–180 °C; yield: 1.41 g (86%); IR<sub>ATR</sub> ( $\nu_{max}/\text{cm}^{-1}$ ): 2900 (C–H), 3300 (NH), 1700 (C=O), 1609 (C=N); UV-Vis (DMSO, 10<sup>-3</sup> M, nm): 268 ( $\pi \rightarrow \pi^*$ ), 311 ( $n \rightarrow \pi^*$ ); <sup>1</sup>H NMR (DMSO-*d*<sub>6</sub>, 500 MHz,  $\delta$  ppm): 11.95 (s, 1H, NH), 8.44 (s, 1H, HC=N), 7.92 (d, 2H, *J* = 7.0 Hz, Aromatic-H), 7.76 (d, 2H, *J* = 7.5 Hz, Aromatic-H), 7.55 (d, 1H, *J* = 7.0 Hz, Aromatic-H), 7.52 (d, 2H, *J* = 7.5 Hz, Aromatic-H), 7.50 (d, 2H, *J* = 7.5 Hz, Aromatic-H); <sup>13</sup>C NMR (DMSO-*d*<sub>6</sub>, 126 MHz,  $\delta$  ppm): 163.19 (1 C, C=O), 146.44 (1 C, C=N), 134.49, 133.32, 133.27, 131.74, 128.87, 128.65, 128.42, 127.60 (Aromatic-C); Anal. Calcd. (%) for C<sub>14</sub>H<sub>11</sub>ClN<sub>2</sub>O (258.0560): C, 65.00; N, 10.83; H, 4.29; Found: C, 64.93; N, 11.06; H, 4.29; MS (*m/z*): Calcd. = 259.0638 [M + H]<sup>+</sup>; Found = 259.0653 [M + H]<sup>+</sup>.

#### Single-Crystal X-Ray Diffraction Analysis

Single crystals of BB2, BB4, and BB6 suitable for data collection were obtained through slow evaporation in methanol over a period of 72 hours. The data collection was performed using APEX II equipped with Mo K $\alpha$  radiation ( $\lambda = 0.71073$ ) at a temperature of 293 K. The collected data was processed using Bruker SAINT software, which integrated the collected frames.<sup>[39]</sup> To mitigate the effects of absorption, SADABS was employed.<sup>[40]</sup> The structures were solved using SHELXT,<sup>[41]</sup> and subsequent structural refinements were conducted using SHELXL.<sup>[42]</sup> Mercury software was utilized to generate graphical representations of the crystals.<sup>[43]</sup> Refinement of the non-hydrogen atoms was carried out on *F*<sup>2</sup> isotropically, followed by anisotropic refinement using the least

squares method. The hydrogen atoms were refined using the riding approximation after being placed geometrically.<sup>[44]</sup>

#### Pharmacological Evaluation

##### Antioxidant Study

##### 2,2'-Diphenyl-1-Picrylhydrazyl (DPPH) Radical Scavenging Assay

The ability of the synthesized compounds to scavenge free radicals was evaluated using the DPPH molecule. The method reported by Turkoglu et al. (2007) was adopted with minor modifications.<sup>[45]</sup> Solutions of the compounds and the positive control (ascorbic acid) were prepared in the concentration range of 125–1000  $\mu\text{M}$ .

To each of these concentrations, 2 mL of a methanolic solution (0.3 mM) of DPPH was added. The resulting mixture was vigorously shaken and kept in a dark chamber at ambient temperature for 30 minutes. Subsequently, the absorbance was measured at a wavelength of 516 nm using a UV-visible spectrophotometer. The ability of the compounds to scavenge the DPPH molecule was estimated as follows:

$$\text{DPPH. Scavenging activity (\%)} = \left( 1 - \frac{\text{Absorbance of compound}}{\text{Absorbance of control}} \right) \times 100$$

##### Ferric Reducing Power (FRAP) Assay

The ferric reducing power of the compounds was assessed using a method reported by Lakshimi.<sup>[46]</sup> A solution of the compounds was prepared with a concentration range of 125–1000  $\mu\text{M}$ .

To 0.75 mL of each concentration, 0.75 mL of phosphate buffer (0.2 M, pH 6.6) was added, followed by the addition of 0.75 mL of K<sub>3</sub>[Fe(CN)<sub>6</sub>] (1%, w/v). The resulting mixture was incubated at 50 °C for 20 minutes. After the incubation period, 0.75 mL of 10% trichloroacetic acid was added. The mixture was then centrifuged at 800 rpm for 10 minutes. The supernatant was removed and mixed with 1.5 mL of water and 1.0 mL of iron (III) chloride (0.1%, w/v). The absorbance of the final solution was measured at 700 nm using a UV-Vis spectrophotometer.

##### Nitric Oxide (NO) Radical Scavenging Assay

To assess the ability of the synthesized compounds to act as antioxidants and scavenge nitric oxide radicals, the modified protocol described by Kurian et al. in 2010<sup>[47]</sup> was employed. In brief, a solution of sodium nitroprusside (10 mM) in potassium phosphate buffer (pH 7.4) was prepared. To 500  $\mu\text{L}$  of the compounds (ranging from 125 to 1000  $\mu\text{M}$ ) or distilled water as a control, 250  $\mu\text{L}$  of the sodium nitroprusside solution was added. The resulting mixture was incubated at 37 °C for 2 hours. After the incubation period, 250  $\mu\text{L}$  of Griess reagent was added to the reaction mixture. The absorbance of the solution was then measured at 546 nm. The percentage of nitric oxide scavenging activity exhibited by the compounds was calculated using a specific formula.

Nitric oxide scavenging (%) =

$$\left(1 - \frac{\text{Absorbance of compound}}{\text{Absorbance of control}}\right) \times 100$$

### Antidiabetic Study

#### $\alpha$ -Glucosidase Inhibition Assay

To evaluate the  $\alpha$ -glucosidase inhibition activity of the synthesized compounds, an in vitro assay was conducted following a literature procedure with slight modifications.<sup>[33]</sup> Concentration series of the synthesized compounds (ranging from 125 to 1000  $\mu$ M) were prepared using dimethyl sulfoxide. In the assay, 50  $\mu$ L of each compound concentration was mixed with 1.0 U/mL of  $\alpha$ -glucosidase. The mixture was preincubated in phosphate buffer (100 mM, pH 6.8) at 37 °C for 15 minutes. Subsequently, a solution of p-nitrophenyl- $\alpha$ -D-glucopyranoside (pNPG) (5 mM, 100  $\mu$ L) in 100 mM phosphate buffer (pH 6.8) was added to the mixture, followed by further incubation for 20 minutes at 37 °C. The absorbance of the reaction mixture was measured at 405 nm, and the obtained results were used to calculate the inhibitory performance of the compounds relative to the positive control (acarbose) using the equation below.

% inhibition =

$$\frac{((A_{405\text{nm}} \text{ of control} - A_{405\text{nm}} \text{ of sample}) \times 100)}{(A_{405\text{nm}} \text{ of control})}$$

#### $\alpha$ -Amylase Inhibition Assay

The  $\alpha$ -amylase inhibition activity of the compounds was assessed following a procedure reported by Shai et al. in 2010, with slight modifications.<sup>[48]</sup> Concentrations ranging from 125 to 1000  $\mu$ M of the compounds were mixed with 2 U/mL of porcine pancreatic amylase and incubated in phosphate buffer (100 mM, pH 6.8) at 37 °C for 10 minutes. Afterwards, a 1% starch solution (50  $\mu$ L) in phosphate buffer (100 mM, pH 6.8) was added to the reaction mixture and further incubated at 37 °C for 10 minutes. Subsequently, 100  $\mu$ L of dinitro salicylate (DNS) color reagent was added to the mixture, which was then boiled for 10 minutes. Acarbose was used as the positive control.

The absorbance of the reaction mixture was measured at 540 nm, and the inhibitory activity was expressed as a percentage of the control using the following formula:

% inhibition =

$$\frac{((A_{405\text{nm}} \text{ of control} - A_{405\text{nm}} \text{ of sample}) \times 100)}{(A_{405\text{nm}} \text{ of control})}$$

### Data Analysis

The data obtained were analyzed using one-way analysis of variance (ANOVA) to determine their statistical significance. The results are presented as mean  $\pm$  standard deviation of the data set, which was obtained from triplicate experiments. To establish the significance difference, Turkey's honestly significant difference (HSD) multiple range post hoc test of GraphPad Prism version 6.01 was employed. The significance level was set at  $p < 0.05$ .

### Computational Study

#### DFT Method

2-dimensional (2D) structures of the hydrazone Schiff bases were drawn using ChemDraw Professional 15.0, a structure modelling program. The 2D structures were converted into 3D using Chem3D,<sup>[49]</sup> a ChemOffice suite used to build, visualize, and analyze 3D models of chemical structures. In Chem3D, each ligand was minimized using the molecular mechanics 2 (MM2) force fields to obtain a structure void of steric effects, arising from disorientation of bonds and non-bonded groups, and their corresponding steric energies.

The minimized structures in SDF format were loaded into Gauss-View program<sup>[50]</sup> and set up for optimization. The popular hybrid density functional theory model B3LYP, reported to have performance superior to other hybrid density functionals and have yielded very good results in several studies<sup>[51,52]</sup> was chosen for the calculations. The basis set to accompany the density functional was determined by exploring the basis set exchange website (<https://www.basissetexchange.org/>). All chemical elements present in the 6 ligands (H, C, O, N, and Cl) were selected for basis set screening. After screening, 689 available basis sets were reduced to 398. Two of the top basis sets in the 398 list, 6-311++G(2d,2p) and 6-311++G(3df,3pd), were chosen for their applicability to H to Br atoms. Both are People-style orbital basis sets (<https://psicode.org/>) with diffuse functions to incorporate, 3d functions and 1f function on heavy atoms, and 2p functions and 1d functions on hydrogen.

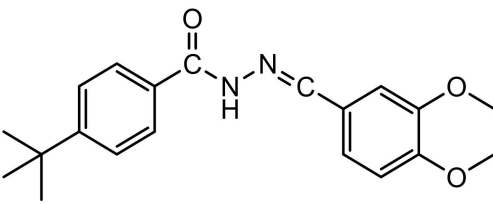
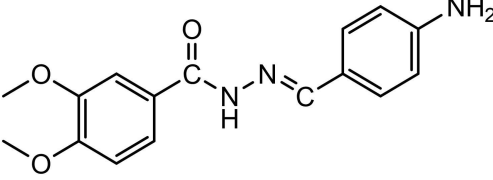
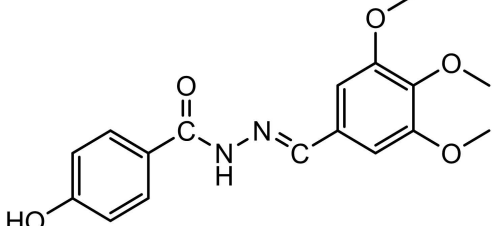
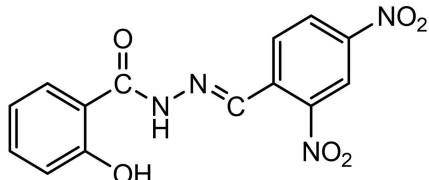
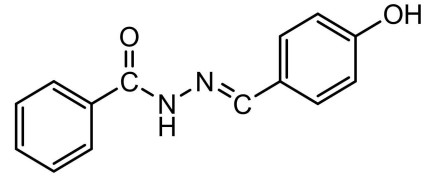
The ligands were first optimized using HF/3-21G method to save computational time and the results were further re-optimized in each of B3LYP/6-311++G(2d,2p) and B3LYP/6-311++G(3df,3pd) methods. The B3LYP/6-311++G(3df,3pd) method gave the lowest optimization energy and was therefore adopted for subsequent calculations. Frequency calculation was carried out to establish the optimized structures are local minima, with all showing no negative imaginary frequencies. Also, single-point energy calculation was carried out to obtain the dipole moment values, as well as quantum chemical descriptors from the check point files, and surfaces/maps for the molecular orbital and electrostatic potential. All calculations were done using the lengau cluster at the center for high performance computing (CHPC) in Cape Town, South Africa.<sup>[T-able 1]</sup>

### Molecular Docking Study

#### Docking Procedures

For each enzyme in the experimental antidiabetic study, two corresponding protein crystal structures were retrieved from the Research Collaboration for Structural Bioinformatics (RCSB) website, <https://www.rcsb.org/>. On  $\alpha$ -amylase, we retrieved proteins with PDB IDs: 2QV4 and 1OSE; while we retrieved proteins with PDB IDs: 2F6D and 2QMJ for  $\alpha$ -glucosidase. Two protein crystal structures were selected for docking in each case to determine the reproducibility of the predicted binding capacity of the novel ligands unto the enzymes. All four proteins each has Acarbose as their native (co-crystallized) ligand in their complexes as deposited in the RCSB website and this is much logical to be used for the molecular docking study since Acarbose is the standard compound in our biological experiment. The macromolecular details of the proteins are presented in Table 2. The protein crystal structures were prepared for docking by stripping them off the co-crystallized ligand, heteroatoms, and water molecules.

**Table 1.** Examples of some biologically active compounds bearing hydrazone moiety.

Compound	Activity	IC <sub>50</sub>	Ref.
	Urease inhibitor	13.42 ± 0.33 μM	[32]
	Antibacterial	26.11 μM	[33]
	Antidiabetic	4.60 ± 2.30	[34]
	AchE inhibitor	0.09 ± 0.01	[35]
	Antioxidant	0.33 ± 0.04 mg/mL	[36]

**Table 2.** Macromolecular details of the proteins.

PDB ID	Name	Resolution (Å)	Study where the protein has been used
2QV4	Human pancreatic α-amylase	1.90	[53]
1OSE	Porcine pancreatic α-amylase	2.30	[54]
2F6D	Glycoamylase from <i>Saccharomycopsis</i>	1.60	[55]
2QMJ	Human intestinal maltase-glucoamylase	1.90	[56]

The 6-311++G(3df,3pd) optimized structures of the Schiff bases and the standard molecule (Acarbose) were each opened in GaussView program and converted to Protein Databank Bank (PDB) format from their LOG file format. Then, Chimera (v1.16) program was employed in adding Gasteiger charges to the ligands. The Gasteiger charge for all Schiff bases is 0 while for Acarbose (both PubChem retrieved and co-crystallized) is -1. The PyRx program, a

virtual screening tool, was used for the docking simulation.<sup>[57]</sup> For docking against protein, the prepared protein was loaded to molecule tab and converted to pdbqt format – an acceptable structure format for docking. Then, all ligands were loaded on the Open Babel interface in PyRx and minimized using the universal force field (UFF) in 200 steps, and then converted to pdbqt format.

Meanwhile, the binding pocket of each protein was earlier determined using Chimera program by opening the co-crystallized ligand in the prepared protein and zoning the ligand within < 5.0 Å distance, to detect interacting amino acids. The region covered by this interacting amino acids defines the binding pocket and it's a measure of the grid box for docking unto the protein binding site. The grid box sizes and dimensions including the component amino acid residues are, for the proteins are tabulated in Table 3.

Prepared ligands in pdbqt formats were loaded from the Vina tab and docked using AutoDock Vina engine embedded in PyRx program. The best fit complex docked pose, having RMSD value 0, out of the 9 runs obtained from each docking simulation was selected and analysed. The separation of retrieved complexes from the RCSB website and analysis of the best fit docked complex was

**Table 3.** Grid box sizes and dimensions, and its component amino acids residues.

	Coordinates of the grid box			Amino acid residues for grid generation
	X	Y	Z	
2QV4 Center	14.2952	49.4059	20.9987	Ile51, Trp58, Trp59, Glu60, Tyr62, Gln63, His101, Gly104, Asn105, Ala106, Val107, Tyr151, Leu162, Thr163, Gly164, Leu165, Arg195, Asp197, Ala198, Lys200, His201, Glu233, Ile235, Asn298, His299, Asp300, His305.
Dimension (Å)	28.4359	25.1410	22.2151	
1OSE Center	36.9995	38.5853	2.2331	Trp58, Trp59, Glu60, Tyr62, Gln63, Val98, His101, Gly104, Ser105, Gly106, Ala107, Tyr151, Gln161, Leu162, Val163, Gly164, Leu165, Arg195, Asp197, Ala198, Lys200, His201, Glu233, Ile235, Glu240, His299, Asp300, His305, Gly306, Ala307.
Dimension (Å)	35.0045	22.1896	27.7754	
2F6D Center	11.5012	7.3078	-8.3409	Ala54, Tyr63, Trp67, Arg69, Asp70, Ala138, Trp139, Gly140, Gln143, Phe206, Leu208, Trp209, Glu210, Glu211, Arg345, Tyr351, Trp362, Glu456, Leu471, Trp473.
Dimension (Å)	20.0069	27.3036	20.5497	
2QMJ Center	-21.2307	-5.8595	-10.3043	Asp203, Thr205, Asn207, Tyr299, Asp327, Ile328, Ile364, Trp406, Trp441, Asp443, Met444, Ser448, Phe450, Arg526, Trp539, Asp542, Thr544, Asp571, Phe575, Ala576, Arg598, His600.
Dimension (Å)	24.7857	20.1003	24.6369	

carried out using Discovery studio visualizer (<https://biovia-discovery-studio-2021-client.software.informer.com/>). The molecular docking procedures are in accordance with those reported by<sup>[58]</sup>

## 2. Results and Discussion

### 2.1. Chemistry

Herein, hydrazone Schiff bases (**BB1–BB6**) have been synthesized using a simple condensation reaction between an equimolar amount of benzohydrazide and benzaldehyde derivatives, using methanol as a solvent in the presence of formic acid as the dehydrating agent as shown in Scheme 1. The compounds were obtained in high yield (80–88%) and purity. All the compounds were isolated as white or grey solid powder, stable in air and moisture. The melting point of the compounds was found to be within the range of 177–240 °C.

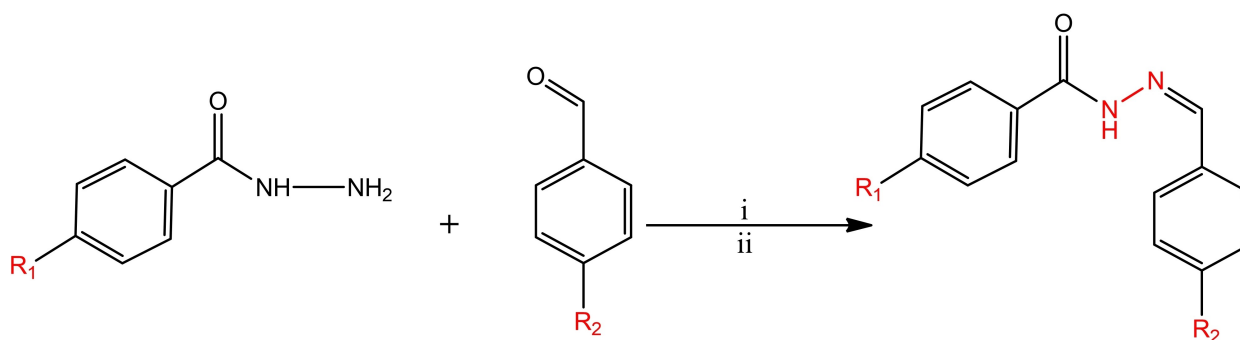
The compounds were characterized using various spectroscopic and analytical techniques, such as FTIR, UV-Vis, elemental (CHN) analysis, NMR (<sup>1</sup>H, <sup>13</sup>C, COSY, NOESY, HMBC, HSQC, and DEPT), and high-resolution mass spectroscopy (HRMS). Based

on the results obtained from the characterization techniques, the structures of the compounds are unequivocally established. Furthermore, single crystals of **BB2**, **BB4**, and **BB6** suitable for data collection were obtained and analyzed. The crystallographic data further affirmed the structures of these compounds. In addition, the data obtained from (HRMS) analysis corroborated well with the calculated molecular mass of the compounds, Table 4.

### 2.2. Spectroscopic Analysis

#### 2.2.1. Nuclear Magnetic Resonance Study

The <sup>1</sup>H and <sup>13</sup>C NMR spectra (1D and 2D) of the compounds (supplementary information) exhibited characteristic peaks that accounted for all the protons and carbons present in the compounds. In the <sup>1</sup>H NMR spectra, a diagnostic singlet peak attributed to the amine protons was observed in the range of 12.15–11.77 ppm. Furthermore, a singlet peak corresponding to one proton of the imine group was detected in the range of 8.54–8.44 ppm in the compound spectra.<sup>[59]</sup> Notably, in the



**Scheme 1.** Reaction pathway for the synthesis of the compounds: i = CH<sub>3</sub>OH/HCOOH; ii = RT/3 hrs; R<sub>1</sub> = H or CH<sub>3</sub>; R<sub>2</sub> = H, Cl or NO<sub>2</sub>.

**Table 4.** Physio-chemical properties of the compounds.

Entry	Color	Yield (%)	m.p. (°C)	Elemental analysis: Calc. (Found)			m/z: [M + H] <sup>+</sup>	
				C	H	N	Calcd.	Found
<b>BB1</b>	White	80	180–183	74.98(74.34)	5.39(5.57)	12.49(12.44)	225.1028	225.1025
<b>BB2</b>	White	82	200–203	62.45(62.58)	4.12(4.12)	15.61(15.68)	270.0879	270.0889
<b>BB3</b>	White	88	236–240	75.61(75.68)	5.92(5.93)	11.76(11.81)	239.1184	239.1207
<b>BB4</b>	Grey	85	220–223	63.60(63.89)	4.63(4.78)	14.83(14.87)	284.1035	284.1064
<b>BB5</b>	Grey	82	210–213	66.06(65.90)	4.80(4.76)	10.27(10.49)	273.0795	273.0817
<b>BB6</b>	white	86	177–180	65.00(64.94)	4.29(4.29)	10.83(11.06)	259.0638	259.0653

spectra of **BB2** and **BB4**, which contain nitro group substituents, these protons appeared at more downfield positions compared to the other compounds. This shift can be attributed to the strong electron-withdrawing nature of the nitro group, leading to proton deshielding and a shift towards the more downfield region of the spectra. Similarly, the aromatic protons were observed in the range of  $\delta$  8.29–7.33 ppm, accounting for all the aromatic protons in the compounds (supplementary information). The influence of the nitro group substituent on the chemical shifts was also evident in the aromatic protons, with the aromatic protons of **BB2** and **BB4** appearing at more downfield positions compared to the other compounds.

In the <sup>13</sup>C NMR spectra of the compounds (supplementary information), peaks in the range of  $\delta$  163–162 ppm were assigned to carbonyl carbon (C=O) functionalities. Additionally, characteristic peaks corresponding to imine carbons were observed in the region of 147–146 ppm. Peaks attributed to aromatic carbons appeared in the range of 142–123 ppm, encompassing all the carbon atoms present in the compounds.

### 2.2.2. Infrared Spectral Analysis

Infrared spectroscopy is a crucial analytical technique for determining the molecular structure and identifying functional groups within a compound. It measures the absorption of infrared light, which corresponds to the vibrational frequencies of chemical bonds.<sup>[60,61]</sup> In this study, infrared spectroscopy was employed to further elucidate the structural orientation of the compounds by identifying various functional groups present. The spectra can be found in the supplementary information. The infrared spectra of compounds **BB1**–**BB6** exhibited significant similarities, displaying characteristic stretching vibrational bands within the following ranges: 1595–1610, 1700–1720, 2700–2900, and 3100–3300 cm<sup>-1</sup>. These bands correspond to C=N, C=O, C–H, and NH functional groups, respectively.<sup>[62,63]</sup> Notably, the spectra of **BB2** and **BB4** exhibited additional stretching vibration bands at 1270–1280 cm<sup>-1</sup> and 1500 cm<sup>-1</sup>, which can be attributed to symmetric and asymmetric vibrations arising from the nitro group.<sup>[64]</sup> These distinct spectral features provided valuable insights into the molecular structure and arrangement of the compounds, contributing to a comprehensive understanding of their chemical properties. [Figure 1].

### 2.2.3. Ultraviolet Visible Spectroscopy

UV-Vis spectroscopy is a valuable tool for identifying functional groups in molecules and understanding their electronic transitions.<sup>[65,66]</sup> In this study, compounds **BB1**–**BB6** were synthesized with different substituents to enhance their biological properties. Although these substituents do not absorb significantly in the UV or visible region, they can influence the absorption characteristics of the aromatic systems by altering electron density and energy levels. Comparative UV-Vis spectral analysis was conducted, and a bathochromic shift relative to **BB1** was observed (Figure 2). The compounds exhibited two absorption maxima with varying wavelengths, indicating different electronic transitions.

Compounds with electron-withdrawing substituents (such as –NO<sub>2</sub>) exhibited higher absorption wavelengths, while those with a combination of electron-donating and electron-withdrawing groups displayed a redshift. The bathochromic shifts were attributed to changes in the molecular environment and electronic structures induced by the substituents. These findings suggest that **BB2**–**BB6** may possess enhanced biological viability compared to **BB1**. However, it is important to note that a molecule's biological properties are influenced by various factors, and while a bathochromic shift can contribute to enhancing those properties, other aspects such as chemical structure and molecular interactions also play significant roles.

### 2.2.4. Mass Spectroscopy

Mass spectrometry is a vital tool in synthetic organic chemistry, providing valuable insights into the identity, structure, purity, and dynamics of organic compounds. This information is crucial for the synthesis and characterization of new molecules.<sup>[67,68]</sup> In the case of the synthesized compounds **BB1**–**BB6**, mass spectrometry was employed to assess their purity and validate their formation. To analyze the compounds, their mass spectra were obtained and are presented in the supplementary information as Figures S16, S32, S47, S61, S77, and S92, respectively. These spectra exhibited a molecular ion peak that closely matched the expected molecular weight of each compound. The results demonstrated remarkable agreement, with a close match between the experimental and theoretical values (Table 4). This consistency strongly suggests that the

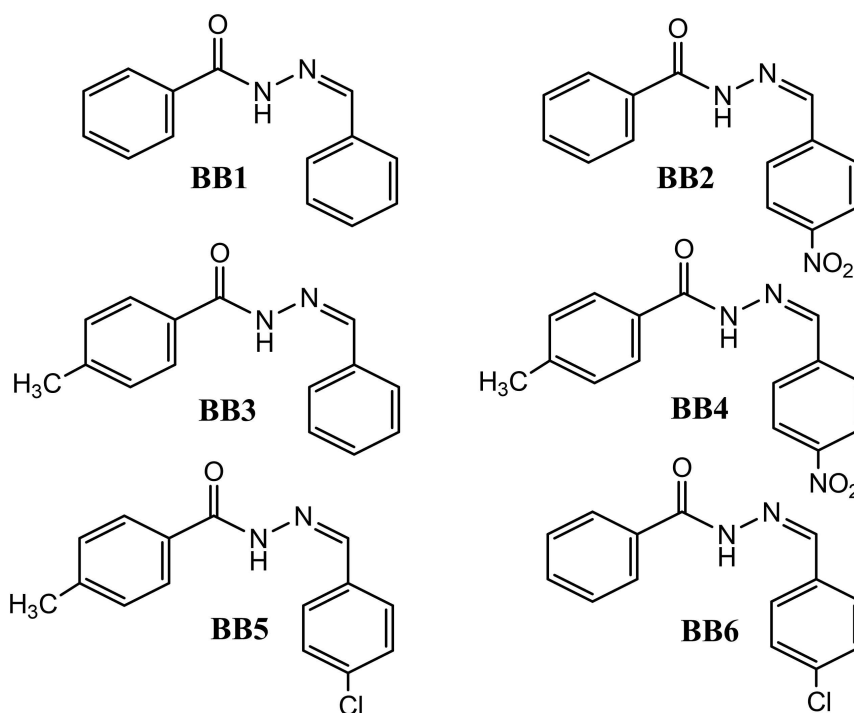


Figure 1. Structures of the synthesized compounds BB1–BB6.

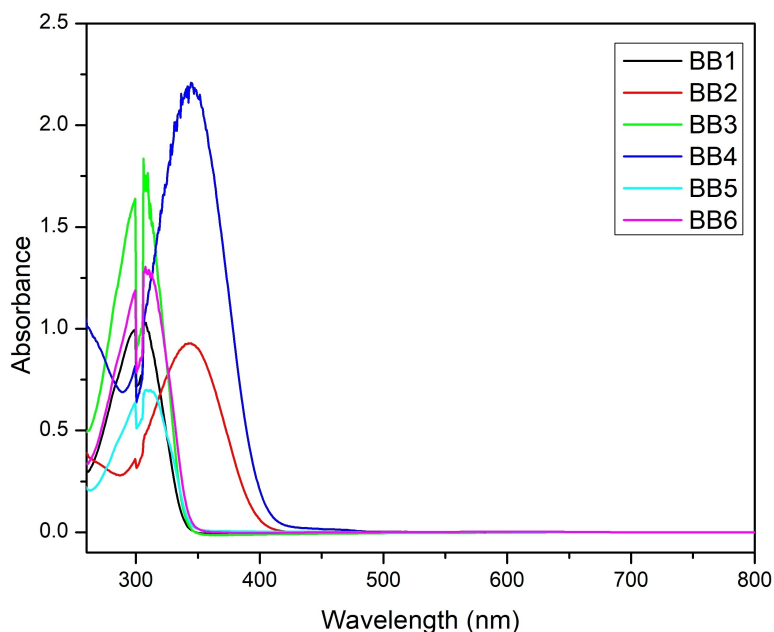


Figure 2. Electronic absorption spectra of the compounds.

compounds were obtained in high purity, indicating the absence of impurities or byproducts. Furthermore, the successful synthesis of the compounds was confirmed by the mass spectrometry results.

#### 2.2.5. Single Crystal X-Ray Diffraction Analysis

Single crystals suitable for data collection for **BB2**, **BB4**, and **BB6** were obtained via slow evaporation in methanol after 72 hours, and the detailed crystallographic data is shown in Table S1. The crystal structures of **BB2** and **BB4** are isomorphs, crystallizing in a monoclinic  $P21/n$  space group, while **BB6** crystallizes in a triclinic  $P-1$  space group. The asymmetric units of all com-



pounds comprise a single molecule that predominantly assumes the *E* conformation. The crystal structure representation of **BB2**, **BB4**, and **BB6** drawn at 50% probability is presented in Figure 3. It is important to note that the asymmetrical unit of **BB4** contains a DMSO molecule that crystallized within the lattice space. The stability of the crystals was confirmed by comprehending intermolecular interactions, specifically focusing on H-bonded interactions since no intramolecular interaction was observed. The stability of **BB4** was aided by the crystallization of DMSO in the asymmetric unit. There exists a non-classical hydrogen bond between the oxygen of DMSO and the nitrogen of the hydrazone  $N(2)-H(2)\cdots O(4)$  (2.143 Å, 160.5°) as depicted in Figure 4. Further analysis of the **BB4** structure revealed that the oxygen of the DMSO forms a tripodal chain involving  $C(9)-H(9)\cdots O(4)$ ,  $C(6)-H(6)\cdots O(4)$ , and  $N(1)-N(2)\cdots O(4)$ . Subsequently, the intermolecular interaction

involving  $N(2)-H(2)\cdots O(1)$  establishes a connection between two molecules positioned on both sides of the asymmetric unit, as well as the neighboring DMSO molecules. The plane of the hydrazine-carbonyl system in **BB4** is more planar (dihedral angle = 13.14(2)°) compared to **BB2** and **BB6**, which have dihedral angles of 33.12(5)° and 38.02(3)°, respectively. Further analysis of the **BB6** packing revealed that the oxygen of the hydrazone forms a 5-membered ring with a neighboring molecule by forming a hydrogen bond with  $C(8)-H(8)\cdots O(1)$  and a van der Waals interaction with  $N(2)-N(1)\cdots O(1)$  (Figure 4). In **BB6**, there exist non-classical interactions between the hydrazone oxygen and the adjacent carbon in the unit cell. The major intermolecular interactions are  $C(5)-H(5)\cdots O(1)$  (3.183 Å) and  $C(6)-O(1)\cdots C(5)$  (Figure 4). All bond angles and bond distances are within the range reported in the literature.<sup>[69–71]</sup>[Figure 5]

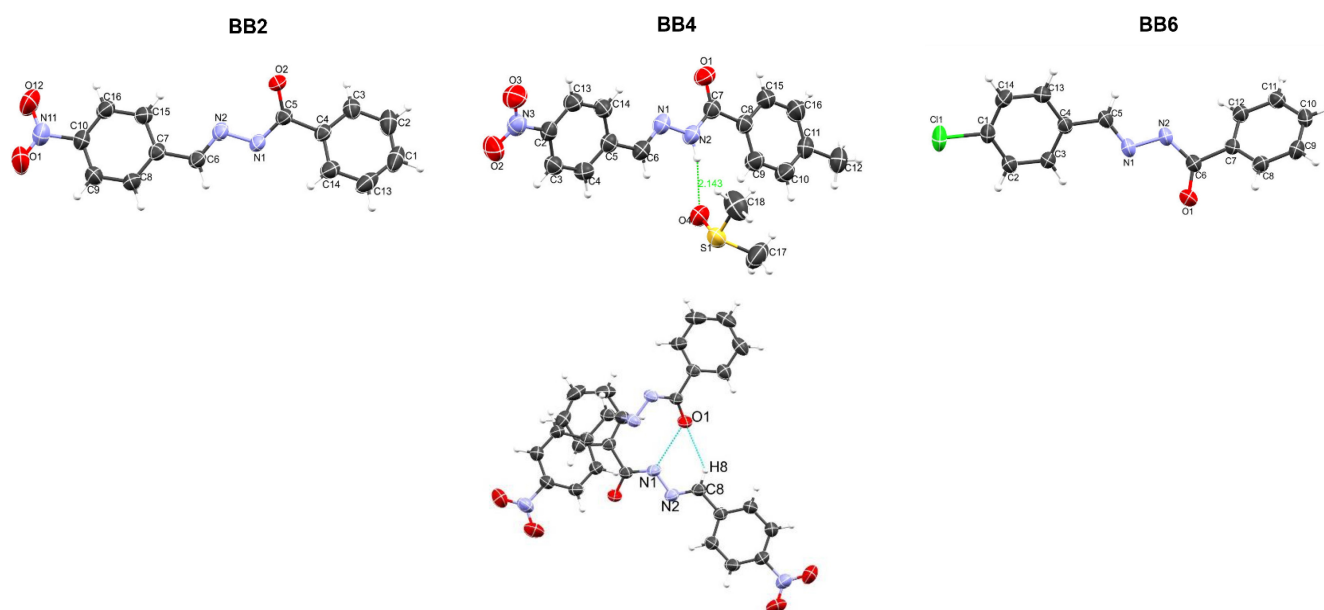


Figure 3. Crystal representation of **BB2**, **BB4**, and **BB6** (Thermal ellipsoid drawn at 50% probability).

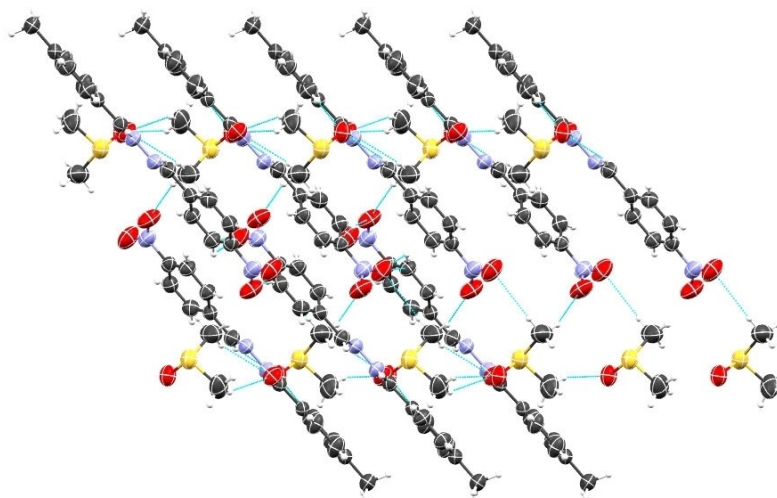


Figure 4. Crystal packing of **BB4** viewed along *b*.

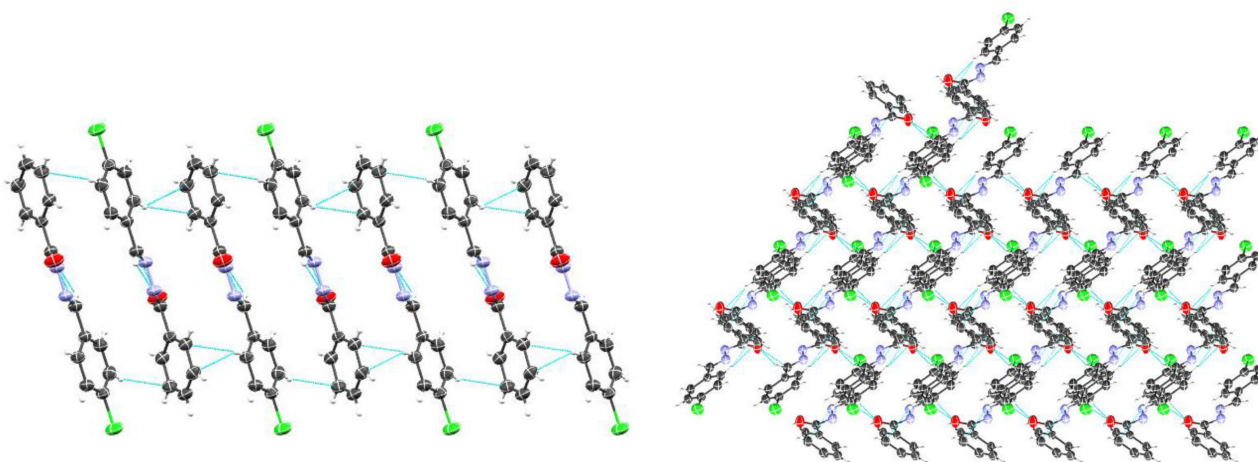


Figure 5. Crystal packing of BB6 viewed along b.

## 2.3. Pharmacological Evaluation and Structural Activity Relation Analysis

### 2.3.1. Antioxidant Study

Oxidative stress is a condition that has harmful effects on living organisms, contributing to the aging process and increasing the risk of developing chronic diseases. This stress occurs when there is an imbalance between the production of reactive oxygen species (ROS) and the body's ability to counteract their damaging effects. Fortunately, oxidative damage can be controlled by antioxidants, substances that play a vital role in scavenging free radicals and inhibiting oxidative reactions. Antioxidants neutralize these highly reactive species, thereby reducing the negative impact of oxidative stress on the body and promoting overall health. Consequently, the chances of developing chronic illnesses are lowered.<sup>[72]</sup> In this study, we evaluated the antioxidant potency of synthesized hydrazone Schiff bases (BB1–BB6) using three different antioxidant assays: DPPH, ferric reducing power, and nitric oxide radical assays. The results of these assays are presented in Tables 5–7 and Figures 6–8.

To fine-tune the biological behavior of the compounds, we strategically designed them with various substituents. These substituents ranged from strong electron-withdrawing ( $-\text{NO}_2$ ) to weak electron-withdrawing (Cl) groups, as well as electron-donating ( $\text{CH}_3$ ) groups. The parent compound, BB1, had no substituents on either of the aromatic rings. BB2 had a nitro group on one ring, BB3 had a methyl substituent, BB4 had a combination of methyl and nitro groups on each ring, BB5 had a combination of methyl and chloride substituents, and BB6 had only a chloride substituent on one of the aromatic rings. The presence of different substituents led to varying degrees of antioxidant activity among the compounds, as observed from the obtained results.

#### 2.3.1.1. 2,2'-Diphenyl-1-Picrylhydrazyl (DPPH) Radical Scavenging Assay

DPPH is commonly used for antioxidant assays because it is a stable free radical compound. When it reacts with an antioxidant, DPPH undergoes a color change from purple to yellow, allowing for the measurement of antioxidant activity using

Table 5. The scavenging rate of the compounds on DPPH radical at various concentration.

	Concentration ( $\mu\text{M}$ )				IC <sub>50</sub>	pIC <sub>50</sub>	LE(kcal/mol)
	125	250	500	1000			
BB1	30.4 ± 1.09	34.5 ± 1.11	38.6 ± 2.50	41.3 ± 2.70	909.1	−3.96	−0.32
BB2	45.6 ± 2.18	48.3 ± 3.18	53.5 ± 2.95	75.8 ± 2.40	551.9	−3.74	−0.25
BB3	37.5 ± 1.02	39.8 ± 2.09	41.6 ± 2.50	48.2 ± 2.50	793.7	−3.90	−0.30
BB4	43.1 ± 3.62	47.3 ± 3.06	51.2 ± 3.97	66.4 ± 4.40	606.1	−3.78	−0.26
BB5	41.3 ± 1.22	44.2 ± 1.02	45.4 ± 2.80	55.4 ± 3.00	708.2	−3.85	−0.28
BB6	40.2 ± 2.68	44.2 ± 2.64	47.5 ± 2.15	59.3 ± 179	670.2	−3.83	−0.29
AA	20.6 ± 2.61	21.6 ± 2.91	21.8 ± 2.41	73.5 ± 40	719.4	−3.86	−0.44

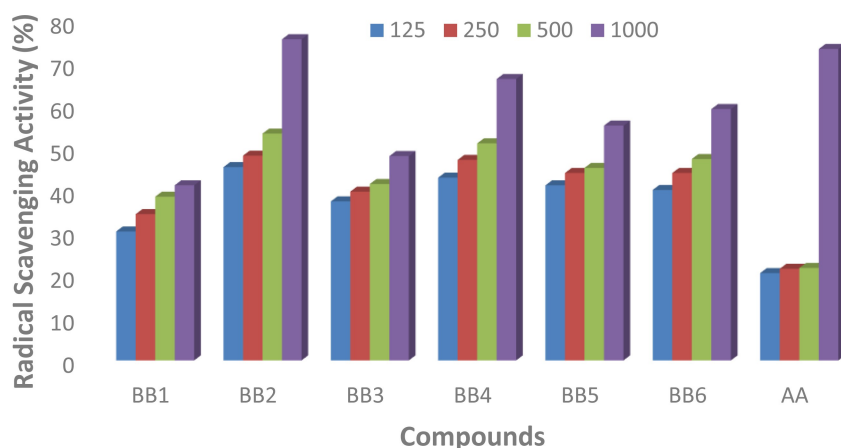
AA stands for ascorbic acid. Values were obtained from three different recording and expressed as mean ± SE; pIC<sub>50</sub> = potency of the antioxidant; IC<sub>50</sub> = concentration at which antioxidant causes 50% scavenging; LE = ligand efficiency.

**Table 6.** The ferric reducing power rate of the compounds at various concentrations.

Entry	Concentration ( $\mu\text{M}$ )				$\text{IC}_{50}$	$\text{pIC}_{50}$	LE(kcal/mol)
	125	250	500	1000			
BB1	$4.1 \pm 0.10$	$4.3 \pm 0.31$	$4.6 \pm 0.12$	$5.0 \pm 0.41$	7463	-4.87	-0.29
BB2	$4.3 \pm 0.41$	$4.9 \pm 0.44$	$5.3 \pm 0.25$	$5.6 \pm 0.36$	6667	-4.62	-0.24
BB3	$4.1 \pm 0.33$	$4.5 \pm 0.53$	$4.8 \pm 0.22$	$5.1 \pm 0.11$	7246	-4.86	-0.27
BB4	$5.6 \pm 0.68$	$5.9 \pm 0.20$	$8.6 \pm 0.30$	$15.0 \pm 0.48$	3086	-4.49	-0.22
BB5	$6.3 \pm 0.48$	$9.7 \pm 0.30$	$12.1 \pm 0.84$	$20.3 \pm 0.73$	2242	-4.35	-0.23
BB6	$4.2 \pm 0.14$	$4.4 \pm 0.32$	$4.7 \pm 0.15$	$5.4 \pm 0.64$	7042	-4.85	-0.27
AA	$33.2 \pm 0.60$	$39.6 \pm 0.41$	$95.1 \pm 0.42$	$101.2 \pm 1.33$	408	-3.61	-0.30

**Table 7.** The nitric oxide radical scavenging activity of the compounds at various concentrations.

Entry	Concentration ( $\mu\text{M}$ )				$\text{IC}_{50}$	$\text{pIC}_{50}$	LE(kcal/mol)
	125	250	500	1000			
BB1	$17.4 \pm 1.41$	$20.7 \pm 2.80$	$23.3 \pm 2.32$	$26.9 \pm 2.54$	1445	-4.16	-0.25
BB2	$23.5 \pm 2.63$	$25.0 \pm 1.42$	$26.3 \pm 1.35$	$29.5 \pm 1.11$	1302	-4.11	-0.21
BB3	$9.1 \pm 2.31$	$20.1 \pm 2.18$	$22.2 \pm 2.09$	$23.9 \pm 2.57$	1612	-4.20	-0.23
BB4	$26.1 \pm 2.63$	$27.6 \pm 2.05$	$29.4 \pm 2.51$	$33.0 \pm 1.53$	1141	-4.01	-0.19
BB5	$3.2 \pm 2.72$	$20.3 \pm 2.41$	$24.1 \pm 3.34$	$27.9 \pm 2.23$	1461	-4.16	-0.22
BB6	$24.3 \pm 1.30$	$25.8 \pm 2.81$	$27.6 \pm 3.91$	$30.6 \pm 3.11$	1231	-4.09	-0.23
AA	$17.1 \pm 2.13$	$28.9 \pm 2.11$	$31.7 \pm 2.62$	$33.9 \pm 2.23$	952	-3.98	-0.33

**Figure 6.** Plot of the DPPH radical scavenging activity of the compounds and the control.

spectrophotometry.<sup>[73]</sup> In this study, the hydrazone Schiff bases (BB1–BB6) also exhibited scavenging activity against DPPH, indicating their potential antioxidant properties. Among the tested compounds, BB2 demonstrated the highest DPPH radical scavenging activity, followed by BB4, BB6, BB5, BB3, and BB1. These compounds exhibited significant scavenging activity at lower concentrations compared to the control (ascorbic acid). BB2 had the lowest  $\text{IC}_{50}$  value, indicating greater potency, and showed the highest  $\text{pIC}_{50}$  and ligand efficiency (LE) values (Table 5 and Figure 6).

The presence of different substituents on the para position of the aromatic rings influenced the scavenging activity of the compounds. Nitro and chlorine substituents, individually or in

combination with methyl groups, enhanced the radical scavenging activity compared to BB1, which had no substituents. Among the compounds, BB4, with a combination of methyl and nitro substituents, exhibited better activity than BB6, BB5, BB3, and BB1. BB2, with a nitro substituent, demonstrated the highest scavenging activity among all the compounds and the control. The control also showed higher scavenging activity at higher concentrations compared to most of the compounds.

In summary, the presence of different substituents on the para position of aromatic rings significantly influenced the biological activity, specifically the radical scavenging activity, of the compounds. Compounds with specific substituents, such as nitro and chlorine, exhibited higher scavenging activity, high-

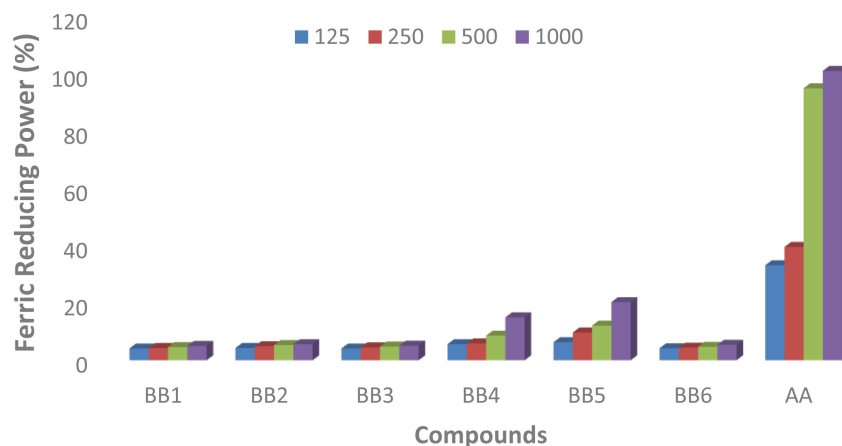


Figure 7. Plot ferric reducing power of the compounds and the control at various concentrations.

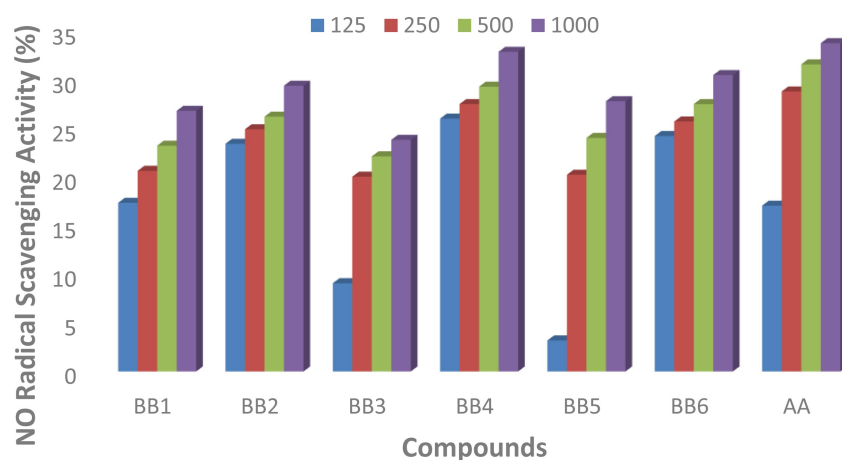


Figure 8. Plot of nitric oxide radical scavenging activity at various concentrations.

lighting the importance of considering substituent effects in drug discovery and antioxidant research. These results align with the findings reported by Taha *et al.*<sup>[74]</sup>

### 2.3.1.2. Ferric Reducing Power (FRAP) Assay

The ferric reducing power assay is a commonly used method to measure the antioxidant capacity of a substance. It determines how well a compound can convert ferric ions ( $\text{Fe}^{3+}$ ) to ferrous ions ( $\text{Fe}^{2+}$ ) through a chemical reaction. Antioxidants have the ability to donate electrons, reducing ferric ions and demonstrating their antioxidant potential.<sup>[75]</sup> The synthesized compounds were evaluated for their ferric reducing power and compared to a control. The results, presented in Table 6 and Figure 7, showed that the compounds had different ferric reducing power compared to their performance in the DPPH radical scavenging assay. However, none of the compounds performed better than the control (ascorbic acid). The control had an  $\text{IC}_{50}$  value of  $408 \mu\text{M}$ , while all the compounds had  $\text{IC}_{50}$  values above  $1000 \mu\text{M}$ . The antioxidant capacity of reducing ferric ions was found to be concentration-dependent, as increasing the

concentrations from 125 to  $1000 \mu\text{M}$  resulted in higher activity. Among the compounds, **BB5** exhibited the highest activity in this assay, surpassing its activity in the DPPH radical scavenging assay. At 1000 and  $125 \mu\text{M}$  concentrations, **BB5** showed reducing rates of  $20.3 \pm 0.73\%$  and  $6.3 \pm 0.4\%$ , respectively. **BB4** also demonstrated significant activity with reducing rates of  $15.0 \pm 0.48\%$  and  $5.6 \pm 0.68\%$  at 1000 and  $125 \mu\text{M}$ , respectively. However, **BB2**, which showed higher radical scavenging activity in the DPPH assay, did not perform as well as **BB5** and **BB6** in the ferric reducing power assay. **BB2** exhibited reducing rates of  $5.6 \pm 0.36\%$  and  $4.3 \pm 0.41\%$  at 1000 and  $125 \mu\text{M}$ , respectively. Similar trends were reported by Sertan *et al.*<sup>[76]</sup> The different activities observed among **BB2**, **BB4**, and **BB5** are due to the nature and electronic properties of the substituents on their aromatic rings. **BB5**, with methyl and chloride substituents, benefits from both groups being electron-donating, increasing the compound's ability to reduce ferric ions. In contrast, **BB4** with a combination of methyl and nitro groups experiences conflicting electronic effects. The electron-withdrawing nature of the nitro group counteracts the reducing power of the methyl group, resulting in lower overall reducing power compared to **BB5**. **BB2**, with only a nitro group, exhibits the

lowest reducing power due to the strong electron-withdrawing properties of the nitro group.

Additionally, **BB6** and **BB3**, which contain only chloride and methyl substituents on their aromatic rings, respectively, displayed moderate activity compared to **BB2**, **BB4**, and **BB5**. This could be attributed to the structural arrangement of the substituents. Having a substituent on only one aromatic ring limits the reducing power to that specific ring, resulting in lower overall reducing capacity compared to compounds with substituents on both rings. Steric hindrance may also affect the accessibility of the compound to ferric ions, further reducing the reducing power. Moreover, **BB1**, without any substituents on its aromatic rings, showed the least activity among all the compounds. It exhibited reducing rates of  $5.0 \pm 0.41\%$  and  $4.1 \pm 0.10\%$  at 1000 and 125  $\mu\text{M}$ , respectively. The absence of electron-donating groups in **BB1** prevents efficient reduction of ferric ions due to the lack of necessary electron density.

In summary, the ferric reducing power of the compounds was influenced by the nature and electronic properties of the substituents on the aromatic rings. Compounds with electron-donating substituents, such as methyl and chloride groups, exhibited higher reducing power, while compounds with electron-withdrawing substituents, such as nitro groups, showed lower reducing power. The absence of substituents or the presence of substituents on only one aromatic ring led to decreased reducing power due to limited electron density and structural arrangement.

### 2.3.1.3. Nitric Oxide (NO) Radical Scavenging Assay

The nitric oxide (NO) radical scavenging assay is performed to evaluate the ability of a substance to scavenge or neutralize nitric oxide radicals. Nitric oxide is a highly reactive molecule that can cause oxidative damage and contribute to various physiological and pathological processes in the body. By assessing the NO scavenging activity of a compound, we can determine its potential to counteract the harmful effects of nitric oxide radicals. Excessive levels of nitric oxide can lead to oxidative stress, inflammation, and tissue damage. Therefore, identifying compounds that can effectively scavenge nitric oxide radicals is important for potential therapeutic applications.<sup>[77]</sup>

In this study, we evaluated the ability of synthesized compounds (**BB1–BB6**) to scavenge nitric oxide radicals compared to a control substance (ascorbic acid) using an *in vitro* assay. The results, shown in Table 7 and Figure 8, revealed that compounds **BB2**, **BB4**, and **BB6** had higher nitric oxide scavenging ability than the control at a concentration of 125  $\mu\text{M}$ . However, compounds **BB1**, **BB3**, and **BB5** did not perform better than the control at the same concentration. Interestingly, as the concentration increased from 250 to 1000  $\mu\text{M}$ , the control showed higher scavenging activity compared to the compounds.

Overall, the scavenging activity of the compounds depended on their concentration. The activity increased as the concentration increased. Compounds **BB2**, **BB4**, and **BB6**

exhibited higher activity compared to **BB1**, **BB3**, and **BB5**. It is worth noting that all the compounds, including the control, had an  $\text{IC}_{50}$  value (concentration at which the activity is reduced by 50%) of more than 1000  $\mu\text{M}$ . The higher activity observed in **BB2**, **BB4**, and **BB6** is likely due to the presence of electron-withdrawing groups. These groups facilitate direct reactions with NO radicals, undergo redox reactions to accept electrons from the radicals, or influence the stability and reactivity of radical intermediates.<sup>[76]</sup>

### 2.3.2. Antidiabetic Study

The need to screen compounds as potential antidiabetic agents arises from the growing prevalence and impact of diabetes worldwide. Due to the complex nature of diabetes and the limitations of current treatments, there is a demand for novel therapeutic approaches. Screening compounds for their potential antidiabetic properties allows for the identification of new drug candidates that can target specific mechanisms involved in diabetes. This screening process involves *in vitro* and *in vivo* testing to evaluate the compounds' efficacy, safety, and pharmacological properties. It is on this note that the synthesized compounds (**BB1–BB6**) were evaluated for their antidiabetic activity using *in vitro*  $\alpha$ -glucosidase and  $\alpha$ -amylase inhibition assays.

#### 2.3.2.1. $\alpha$ -Glucosidase Inhibition Assay

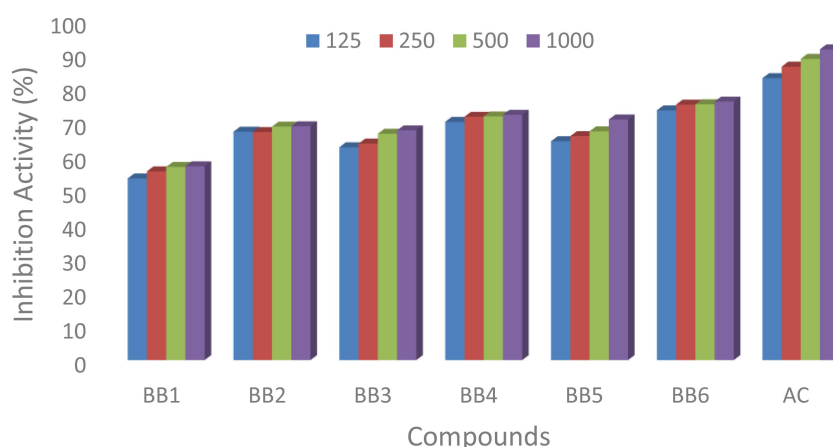
$\alpha$ -glucosidase inhibition assay is a valuable tool in evaluating the potential of compounds as antidiabetic agents. It assesses their ability to inhibit the activity of  $\alpha$ -glucosidase, an enzyme involved in carbohydrate digestion. Compounds demonstrating significant  $\alpha$ -glucosidase inhibition have the potential to regulate postprandial blood glucose levels and may serve as candidates for further development as antidiabetic drugs. It helps to identify compounds with promising antidiabetic activity for further optimization.<sup>[53,78]</sup> The antidiabetic activity of hydrazone Schiff base derivatives (**BB1–BB6**) was evaluated by measuring their ability to inhibit the  $\alpha$ -glucosidase enzyme, with acarbose used as a control. Table 8 and Figure 9, shows that all the compounds exhibited moderate to good inhibition of  $\alpha$ -glucosidase, ranging from  $53.6 \pm 2.02\%$  to  $57.2 \pm 2.36\%$ . Among these compounds, **BB2**, **BB4**, **BB5**, and **BB6**, which contain electron-withdrawing groups ( $-\text{NO}_2$  or  $-\text{Cl}$ ) at the para position, demonstrated relatively stronger inhibition compared to other derivatives. **BB1**, without any substituent, showed the weakest inhibition activity against the  $\alpha$ -glucosidase enzyme. Similarly, **BB3**, with an electron-donating (methyl) group, exhibited higher activity than **BB1** but lower than **BB2**, **BB4**, **BB5**, and **BB6**. In summary, the order of activity for the compounds can be represented as **BB6** > **BB4** > **BB2** > **BB5** > **BB1**.

The modification of the hydrazone derivatives by introducing methyl, nitro, chloride, a combination of methyl and nitro, or methyl and chloride at the *para* position of the aromatic

**Table 8.** The  $\alpha$ -glucosidase inhibition activity of the compounds at various concentrations.

Entry	Concentration ( $\mu$ M)				IC50	pIC50	LE(kcal/mol)
	125	250	500	1000			
BB1	53.6 $\pm$ 2.02	55.7 $\pm$ 2.77	57.0 $\pm$ 2.30	57.2 $\pm$ 2.36	198.21	-3.29	-0.19
BB2	67.4 $\pm$ 0.66	67.3 $\pm$ 1.11	68.9 $\pm$ 2.22	69.0 $\pm$ 1.50	71.76	-2.85	-0.14
BB3	62.8 $\pm$ 1.30	63.9 $\pm$ 1.13	66.8 $\pm$ 1.96	67.8 $\pm$ 1.88	88.09	-2.94	-0.16
BB4	70.3 $\pm$ 2.16	71.8 $\pm$ 2.57	71.9 $\pm$ 1.55	72.4 $\pm$ 2.80	57.32	-2.75	-0.13
BB5	64.6 $\pm$ 2.30	66.1 $\pm$ 2.96	67.5 $\pm$ 2.25	71.0 $\pm$ 3.29	76.60	-2.88	-0.15
BB6	73.7 $\pm$ 1.93	75.4 $\pm$ 2.20	75.5 $\pm$ 2.22	76.3 $\pm$ 2.85	46.43	-2.66	-0.14
AC	83.2 $\pm$ 0.99	86.6 $\pm$ 1.29	88.9 $\pm$ 1.10	91.7 $\pm$ 0.39	26.21	-2.40	-0.20

Note: AC=Acarbose.

**Figure 9.** Plot of  $\alpha$ -glucosidase inhibition activity of the compounds at various concentrations.

rings improved their activity.<sup>[79]</sup> For example, when comparing **BB2**, which has a nitro substituent at the *para* position, to **BB1** without any substituent, at a concentration of 125  $\mu$ M, **BB1** inhibited 53.6 $\pm$ 2.02% of the  $\alpha$ -glucosidase enzyme, while **BB2** inhibited 67.4 $\pm$ 0.66% at the same concentration. Similarly, at 1000  $\mu$ M, **BB1** exhibited 57.2 $\pm$ 2.36% inhibition, whereas **BB2** showed 69.0 $\pm$ 1.50%. These modifications have yielded the desired results and provide opportunities for further optimization and evaluation of the compounds.

### 2.3.2.2. $\alpha$ -Amylase Inhibition Assay

The assay provides valuable information about the inhibitory potency and selectivity of a compound towards  $\alpha$ -amylase. It helps to identify compounds with promising antidiabetic activity and can guide the optimization of drug candidates with improved efficacy, potency, and safety profiles.<sup>[53,78]</sup> Considering this, we evaluated the antidiabetic activity of synthesized hydrazone Schiff base derivatives (**BB1**–**BB6**) using an  $\alpha$ -amylase enzyme inhibition assay, with acarbose used as a reference standard. The results obtained from this study are presented in Table 9 and Figure 10. Accordingly, the compounds exhibited varying degrees of  $\alpha$ -amylase inhibition activity, with inhibition rates ranging from 43.4 $\pm$ 0.67% to 54.8 $\pm$ 0.47% at lower and

higher concentrations, respectively. The inhibition activity of the compounds against  $\alpha$ -amylase was found to be concentration-dependent, like the results observed in other assays conducted on these compounds. Among the compounds, **BB2** and **BB4**, which have nitro substitutions, showed higher inhibition activity. They were followed by **BB5** and **BB6**, which have chloro substitutions, and **BB3**, which has a methyl substitution. **BB1**, which is unsubstituted, exhibited the lowest inhibition activity. This trend was consistent across all the assays conducted on the compounds.<sup>[79]</sup>

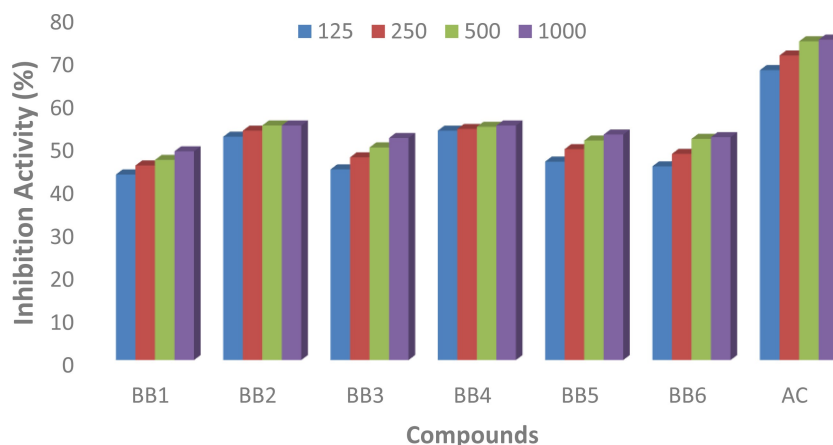
The variation in substitution and increased electronic properties of the compounds played a significant role in determining their inhibition activity. Like the  $\alpha$ -glucosidase inhibition assay, the modification of compounds from **BB2** to **BB6** led to improved activities, with **BB4** displaying higher inhibition due to the combination of electron-donating and electron-withdrawing groups. In general, the order of inhibition activity among the compounds can be represented as **BB4** > **BB2** > **BB5** > **BB6** > **BB3** > **BB1**.

### 2.4. Structural Activity Relationship

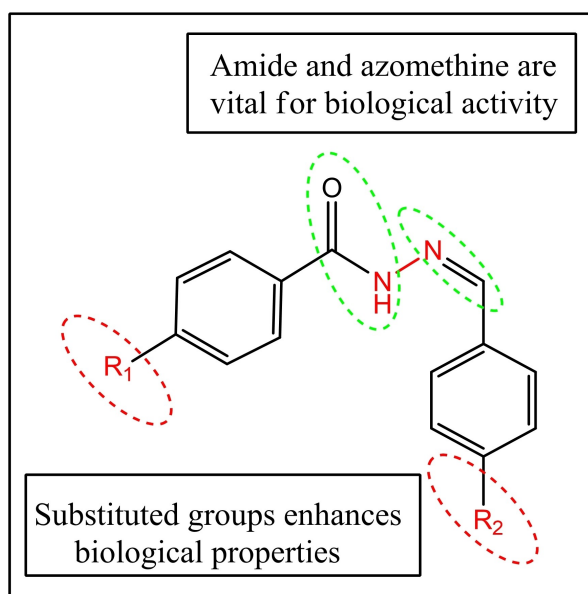
In order to assess the impact of substituent groups and functional groups on the biological properties of the synthe-

**Table 9.** The  $\alpha$ -amylase inhibition activity of the compounds at various concentrations.

Entry	Concentration ( $\mu\text{M}$ )				IC50	pIC50	LE (kcal/mol)
	125	250	500	1000			
BB1	43.4 $\pm$ 0.67	45.5 $\pm$ 0.12	46.8 $\pm$ 0.48	48.8 $\pm$ 0.40	452.95	-3.63	-0.21
BB2	52.2 $\pm$ 0.80	53.6 $\pm$ 0.39	54.8 $\pm$ 0.15	54.8 $\pm$ 0.47	245.74	-3.39	-0.17
BB3	44.6 $\pm$ 0.39	47.4 $\pm$ 0.64	49.7 $\pm$ 1.26	51.9 $\pm$ 0.57	441.41	-3.64	-0.20
BB4	53.6 $\pm$ 0.19	54.0 $\pm$ 0.39	54.5 $\pm$ 0.10	54.8 $\pm$ 0.46	239.66	-3.38	-0.16
BB5	46.4 $\pm$ 1.08	49.3 $\pm$ 0.16	51.3 $\pm$ 0.95	52.7 $\pm$ 0.32	553.30	-3.74	-0.15
BB6	45.3 $\pm$ 1.40	48.2 $\pm$ 0.46	51.7 $\pm$ 0.47	52.1 $\pm$ 0.39	443.06	-3.65	-0.20
AC	67.7 $\pm$ 0.42	71.1 $\pm$ 0.79	74.4 $\pm$ 0.43	74.8 $\pm$ 0.16	56.77	-2.75	-0.22

**Figure 10.** Plot of  $\alpha$ -amylase inhibition activity of the compounds at various concentrations.

sized compound, a study was conducted on the structural activity relationship (Figure 11). Previous literature reports<sup>[15,80–83]</sup> have indicated that the presence of electron withdrawing,

**Figure 11.** Structural activity relationship of the compounds;  $R_1 = \text{H}$  or  $\text{CH}_3$ ;  $R_2 = \text{H}$ ,  $\text{Cl}$  or  $\text{NO}_2$ .

electron donating, and halogen groups can significantly influence the biological properties of compounds. Building upon this knowledge, the current research project was conceived with the aim of synthesizing and evaluating compounds **BB1–BB6**, which contain these specific groups, to determine and compare their pharmacological properties. The *in vitro* pharmacological assays revealed distinct activity profiles among the compounds. **BB4** displayed the highest activity across all the assays conducted. This compound featured both a nitro group and a methyl group as substituents on the para position of the aromatic rings. The presence of these specific substituents significantly enhanced the compound's biological properties, leading to improved antioxidant and antidiabetic activities.

**BB2**, which possessed a nitro group on the para position of one of the aromatic rings, exhibited considerable activity in the assays. Although slightly lower than **BB4**, the nitro group contributed to the observed biological effects of the compound.

**BB5** contained a methyl group and a chloride group as substituents on the para position of the aromatic rings. It displayed moderate activity in the conducted assays, indicating that these specific substituents exerted a moderate influence on the compound's biological properties.

Conversely, **BB6**, with chlorine substituents solely on the para position of one of the aromatic rings, exhibited lower

activity compared to **BB5**. This suggests that the presence of a single chlorine substituent had a lesser impact on the compound's biological effects.

**BB3**, featuring only a methyl group as a substituent on the para position of one of the aromatic rings, demonstrated lower activity compared to **BB5** and **BB6**. Thus, the presence of a single methyl substituent had a minimal effect on the compound's biological properties.

**BB1**, lacking any substituents on either of the aromatic rings, was found to be the least active among all the synthesized compounds. The absence of substituents limited its biological activity in the conducted assays.

The observed trends in the compound activities based on their specific substituents underscore the significance of these substituents on the aromatic rings in modulating the biological properties of hydrazone compounds. These findings were further supported by computational and molecular docking studies, which validated the experimental results.

## 2.4. Computational Study

### 2.4.1. Steric and Optimization Energies

The energies associated with overcoming of the steric hinderances of the Schiff bases as well as their optimization energies at various basis sets are presented in Table 10. **BB6** has the highest steric energy (6.211 kcal/mol) followed by **BB5** (6.091 kcal/mol) and this can be attributed to the large repulsion between the Cl atom and its adjacent H atoms due to the wide electro-

negativity difference. In addition, the B3LYP/6-311++G(3df,3pd) method gave the lowest energy of optimization when compared to other methods, and Schiff base **BB5** has the least optimization energy.

### 2.4.2. Quantum Chemical Descriptors

The quantum chemical descriptors determined from the single-point energy calculations include dipole moment and energies of the highest occupied molecular orbital ( $E_{\text{HOMO}}$ ) and lowest unoccupied molecular orbital ( $E_{\text{LUMO}}$ ). The fundamental quantum chemical descriptors HOMO and LUMO were used to evaluate the values for other descriptors using the following Equations (1)–(8), and the quantum chemical descriptors for each of the compound are presented in Table 11.

$$\Delta E = E_{\text{LUMO}} - E_{\text{HOMO}} \quad (1)$$

$$I = -E_{\text{HOMO}} \quad (2)$$

$$A = -E_{\text{LUMO}} \quad (3)$$

$$\eta = \frac{\Delta E}{2} \quad (4)$$

$$\delta = \frac{1}{\eta} \quad (5)$$

$$\chi = \frac{(I + A)}{2} \quad (6)$$

**Table 10.** Steric and optimization energies of the Schiff base molecules.

Entry	Steric energy (kcal/mol)	Optimization energy (Hartree)		
		HF/3-21G	B3LYP/6-311++G(2d,2p)	B3LYP/6-311++G(3df,3pd)
<b>BB1</b>	5.416	-716.850	-725.636	-725.665
<b>BB2</b>	5.861	-919.139	-930.203	-930.241
<b>BB3</b>	5.302	-755.672	-764.966	-764.996
<b>BB4</b>	5.301	-957.961	-969.533	-969.572
<b>BB5</b>	6.091	-1212.385	-1224.590	-1224.623
<b>BB6</b>	6.211	-1173.563	-1185.260	-1185.292

**Table 11.** Calculated quantum chemical descriptors for the Schiff bases.

Entry	ELUMO	EHOMO	$\Delta E$	I	A	$\eta$	$\delta$	$\chi$	Cp	$\omega$	$\mu\text{D}$
<b>BB1</b>	-1.83	-6.60	4.77	6.60	1.83	2.38	0.41	4.21	-4.21	3.72	3.58
<b>BB2</b>	-3.25	-7.09	3.84	7.09	3.25	1.92	0.52	5.17	-5.17	6.96	5.02
<b>BB3</b>	-1.78	-6.54	4.75	6.54	1.78	2.37	0.42	4.16	-4.16	3.64	3.35
<b>BB4</b>	-3.22	-7.03	3.81	7.03	3.22	1.90	0.52	5.12	-5.12	6.89	5.64
<b>BB5</b>	-1.97	-6.60	4.62	6.60	1.97	2.31	0.43	4.29	-4.29	3.98	3.32
<b>BB6</b>	-2.02	-6.66	4.64	6.66	2.02	2.32	0.43	4.34	-4.34	4.06	3.19
<b>Aca</b>	-0.83	-5.76	4.92	5.76	0.83	2.46	0.40	3.29	-3.29	2.20	3.65

All units are in eV except  $\mu\text{D}$  (Debye).  $\Delta E$ : Energy gap A: Electron affinity, I: Ionization potential,  $\eta$ : Global hardness,  $\delta$ : Global softness,  $\chi$ : Electronegativity, Cp: Electronic chemical potential,  $\omega$ : Global electrophilicity,  $\mu\text{D}$ : Dipole moment.



$$C_p = -\chi \quad (7)$$

$$\omega = \frac{\chi^2}{\Delta E} \quad (8)$$

The energy gap between LUMO and HOMO,  $\Delta E$ , quantifies the chemical reactivity of the molecules (Yusuf, *et al.*, 2021). Meanwhile,  $\Delta E$  also describes the stability of a given compound (Uesugi, *et al.*, 1997), in an inverse proportion. Thus, a more stable compound is less reactive while a less stable compound is more chemically reactive. As seen from Table 10, **BB1** has the highest  $\Delta E$  value (4.77 eV), among the novel compounds, implying that it is the most stable and least chemically reactive. On the other hand, **BB4** with the lowest  $\Delta E$  value (3.81 eV) is the least stable and the most chemically reactive. The order of chemical reactivity of the Schiff bases will therefore be **BB4** < **BB2** < **BB5** < **BB6** < **BB3** < **BB1**. The reduced stability of **BB4** and **BB2**, with  $\Delta E$  values 3.81 and 3.84 eV, respectively; leading to their high chemical reactivity can be attributed to the presence of the electron withdrawing group  $\text{NO}_2$ . The  $\text{NO}_2$  substituent concentrates positive charges towards the *ortho* and *para* positions of the aromatic ring and makes the positions deactivated towards electrophilic aromatic substitution. Meanwhile, the reference molecule, Acarbose (**Aca**), has higher  $\Delta E$  value (4.92 eV) suggesting it is less chemically reactive compared to the novel compounds.

These **BB2** and **BB4** molecules also show strong electrophilicity by their high ionization energies (I), 7.09 and 7.03 eV, respectively. Similarly, they both have high electron affinity (A) values 3.25 and 3.22, respectively. Thus, these molecules are electrophilic and would be highly chemically reactive, rendering the aromatic system susceptible to electrophilic substitution. The global hardness,  $\eta$ , quantitatively measures resistance to charge transfer while the global softness,  $\delta$ , measures susceptibility to charge transfer.<sup>[84,85]</sup> Therefore, **BB2** and **BB4** Schiff bases with low  $\eta$  values (1.92 and 1.90 eV) and high  $\delta$  values (~0.52 eV for both) are softer than other compounds, susceptible to charge transfer and more chemically reactive than their counterparts. The dipole moment,  $\mu_D$ , quantifies the electron distribution within a molecule and describes the distance between two opposite charges.<sup>[86]</sup> From Table 10, **BB2** and **BB4** have high  $\mu_D$  values 5.02 and 5.64 Debye, respectively; and these can be attributed to highly electronegative  $\text{NO}_2$  substituent.  $\text{NO}_2$  is a highly electronegative group,<sup>[87]</sup> making a cloud of electrons concentrated on nitroaromatic ring and therefore conferring a significant partial distribution of electron on the system.

### 2.4.3. Frontier Molecular Orbitals

The frontier molecular orbital (FMO) maps describe the way molecules interact with surrounding substances be it metal ions or biological targets.<sup>[88]</sup> The FMO maps for the Schiff bases are presented in Figure 12. Since all the novel compounds are similar, having **BB1** as the basic structure and only differ in

substituents, an IUPAC name *N'*-benzylidenebenzohydrazide was obtained for **BB1** using ChemDraw® Professional v15.0 program, to guide in understanding the positions of substituents and the structural make ups of the compounds. **BB1**, **BB3**, **BB5** and **BB6** have contribution to their LUMOs from both the *N'*-benzylidene and the benzohydrazide groups, while **BB2** and **BB4** have contributions to their LUMOs dominantly from only the *N'*-benzylidene moiety and the amide -CONH chain of the benzohydrazide group. All six Schiff bases have contributions to their HOMO from the *N'*-benzylidene moiety and its substituents, as well as from the amide -CONH chain of the benzohydrazide group.

### 2.3.4. Molecular Electrostatic Potential Maps

The molecular electrostatic potential (MEP) map is a 3-dimensional surface useful for gaining insights into the charge distribution and reactivity of chemical molecules.<sup>[89]</sup> Also, the MEP map has been reported as an electron density-based descriptor for predicting and analyzing a molecule's nucleophilic and nucleophilic sites of reactivity.<sup>[90]</sup>

The blue region indicate areas of positive electrostatic potential and sites of electrophilic reactivity while red regions are areas of negative electrostatic potential and sites of nucleophilic reactivity.<sup>[91]</sup> As shown in Figure 13, for all the Schiff bases, the sites of electrophilic reactivity ranges from the -NH-N chain of the benzohydrazide group to the *N'*-benzylidene moiety. The sites of electrophilic reactivity are the C=O and benzyl moiety of the benzohydrazide group for all, and the  $\text{NO}_2$  substituent of *N'*-benzylidene group for **BB2** and **BB4**. The additional site of electrophilic reactivity observed for **BB2** and **BB4** can be associated with increased chemical reactivities in them as evident in their energy gap values. As for the reference molecule, Acarbose (**Aca**), the sites of electrophilic reactivity are localized on hydroxyl O atoms, the methyl and the amine groups. On the other hand, its sites of nucleophilic reactivity are localized on the oxygen atoms, both hydroxy and oxo groups.

### 2.5. Molecular Docking Analysis

The molecular information including formulae, molecular weight, number of atoms and minimization energy are presented in Table 12. The energy minimization enhances reduction of the overall potential energy of the ligand, making the energy minimized ligand to provide clear idea of the active site residue orientation as well as the active site cavity size.<sup>[92]</sup> **BB2** and **BB4** require greater energies for minimization, and these could be attributed to the presence of  $\text{NO}_2$  substituent in them. Notably,  $\text{CH}_3$  substituent is also observed to make a difference (about 2–3 energy increase) in the minimization energy as seen when **BB1** and **BB3**, **BB2** and **BB4**, and **BB5** and **BB6** pairs are compared. This is so because the three H atoms of  $\text{CH}_3$  require additional energy to attain the proper molecular

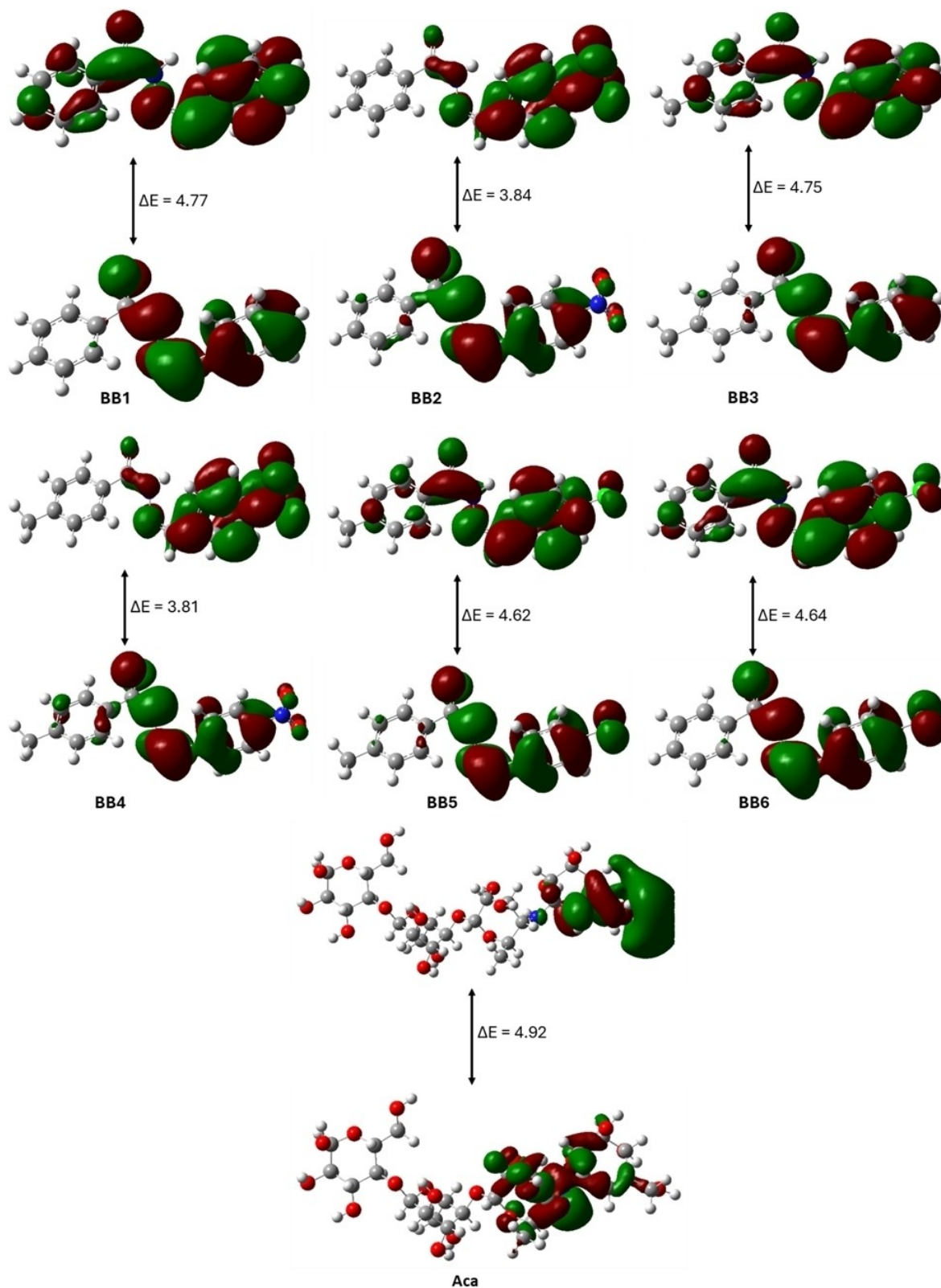
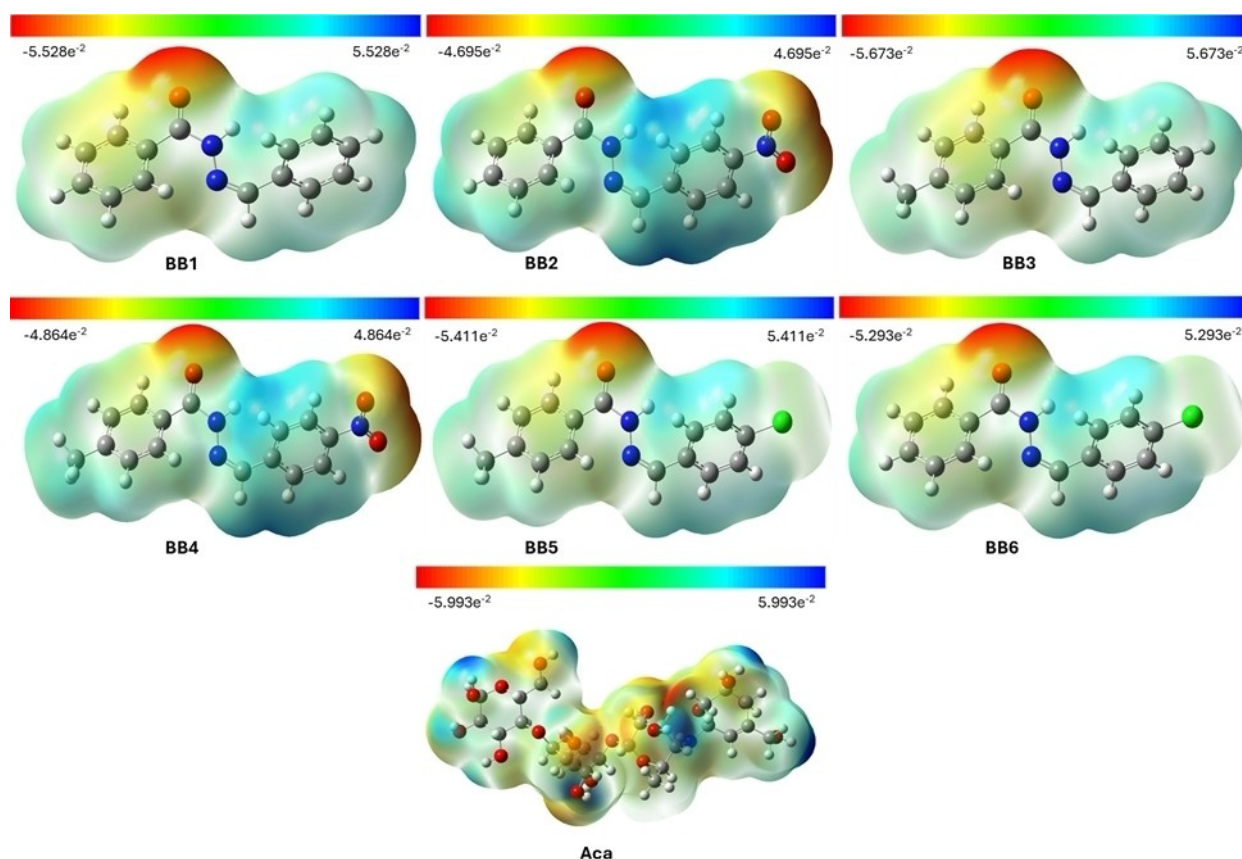


Figure 12. Frontier molecular orbital maps of BB1–BB6 and Aca, predicted by 6-311 + g(3d,3pd) basis set with DFT/B3LYP functional using Gaussian 16 vB01.

arrangements in space from the drawn non-favorable energetic chemical structure.

Molecular docking is described as a computational modeling approach for the prediction of preferred binding orientation of a molecule, usually ligand, to another molecule, usually



**Figure 13.** Molecular electrostatic potential maps of BB1–BB6 and Aca, predicted by 6-311 + g(3d,3pd) basis set with DFT/B3LYP functional using Gaussian 16 vB01. The electron-rich and poor regions are shown in colours red–orange–yellow–green–blue.

**Table 12.** Molecular information and binding energies of the ligands.

	Formula	Weight (g/mol)	No. of atoms	Min. Energy	Binding energies (kcal/mol)			
					1OSE	2QV4	2F6D	2QMJ
<b>BB1</b>	C <sub>14</sub> H <sub>12</sub> N <sub>2</sub> O	224.25	29	272.13	−7.5	−7.4	−8.8	−6.7
<b>BB2</b>	C <sub>14</sub> H <sub>11</sub> N <sub>3</sub> O <sub>3</sub>	269.25	31	294.22	−8.0	−7.9	−8.8	−6.9
<b>BB3</b>	C <sub>15</sub> H <sub>14</sub> N <sub>2</sub> O	238.28	32	275.11	−7.8	−7.8	−8.9	−7.5
<b>BB4</b>	C <sub>15</sub> H <sub>13</sub> N <sub>3</sub> O <sub>3</sub>	283.28	34	296.80	−8.4	−8.1	−8.3	−6.8
<b>BB5</b>	C <sub>15</sub> H <sub>13</sub> ClN <sub>2</sub> O	272.72	32	274.15	−8.1	−7.7	−8.8	−6.7
<b>BB6</b>	C <sub>14</sub> H <sub>11</sub> ClN <sub>2</sub> O	258.70	29	270.93	−7.8	−7.8	−8.9	−6.9
<b>Aca</b>	C <sub>25</sub> H <sub>43</sub> NO <sub>18</sub>	645.60	87	920.07	−7.6	−7.6	−7.7	−6.4

Aca = acarbose.

receptor, when they both interact to form a stable complex.<sup>[93]</sup> Different conformers generated during molecular docking are scored and compared with each other, and the best docked conformer/pose having RMSD value of 0 are accepted.<sup>[94]</sup> The binding score (energy) obtained for the best docked pose for all ligand-protein complexes are presented in Table 10.

For  $\alpha$ -amylase proteins, **BB4** showed the highest inhibition capacity (−8.4 and −8.1 kcal/mol for 1OSE and 2QV4, respectively) while **BB1** has the least capacity (−7.5 and −7.4 kcal/mol for 1OSE and 2QV4, respectively). Overall, All the Schiff bases,

except **BB1**, demonstrated lower binding affinity and greater inhibition against  $\alpha$ -amylase than the standard ligand.

For  $\alpha$ -glucosidase, **BB3** showed the highest inhibition capacity (−8.9 and −7.5 kcal/mol for 2F6D and 2QMJ, respectively). All Schiff bases demonstrated lower binding energy and greater inhibition against  $\alpha$ -glucosidase than the standard ligand. The molecular docking simulations have shown reliability by giving similar results trend for the same protein belonging to a specific cell line. These results help in achieving the aim of using two proteins to test the reproducibility of the

predicted binding capacity of the novel ligands unto enzymes of the same infection.

2D diagram showing the amino acid residues involved in the receptor-ligand interactions between protein and the standard compound and the most effective Schiff base for each category are presented in Figures 14–17. For  $\alpha$ -amylase proteins (Figures 14 and 15), the interactions common to the standard drug in both proteins include van der Waals, conventional hydrogen bond, unfavorable donor-donor interactions. In addition, unfavorable acceptor-acceptor and pi-donor hydrogen bond interactions were observed for porcine  $\alpha$ -amylase protein. BB4 interacts with both  $\alpha$ -amylase proteins having van der Waals, conventional hydrogen bond, pi-pi stacked alkyl interactions in common. Pancreatic  $\alpha$ -amylase protein has additional interactions including carbon hydrogen bond, pi-cation, pi-anion, and pi-alkyl interactions.

For  $\alpha$ -glucosidase proteins (Figures 16 and 17), the interactions common to the standard drug in both proteins are van

der Waals and conventional hydrogen bond interactions. Pi-donor hydrogen bond interaction was observed as an addition for human maltase-glycoamylase protein. BB3 interact with both  $\alpha$ -glucosidase proteins having van der Waals, attractive charge, pi-anion, pi-pi T-shaped and pi-alkyl interactions in common. The human maltase-glycoamylase protein has pi-sigma interaction as an additional interaction.

Furthermore, here is a juxtaposition of the top performing reported molecule with a reference co-crystallized ligand of the protein to gain insights into their interactions. The binding energies of the co-crystallized ligand of 2QV4 and BB4 ligand when docked unto the protein are  $-9.1$  and  $-8.1$ , respectively. These suggest that the co-crystallized ligand have stronger affinity for the protein binding site and inhibits the binding pocket of alpha-amylase more strongly than the top performing ligand molecule. The interactions are presented in Figure 18. Notably, both molecules interact with the protein strongly, having some amino acids residues in common but with

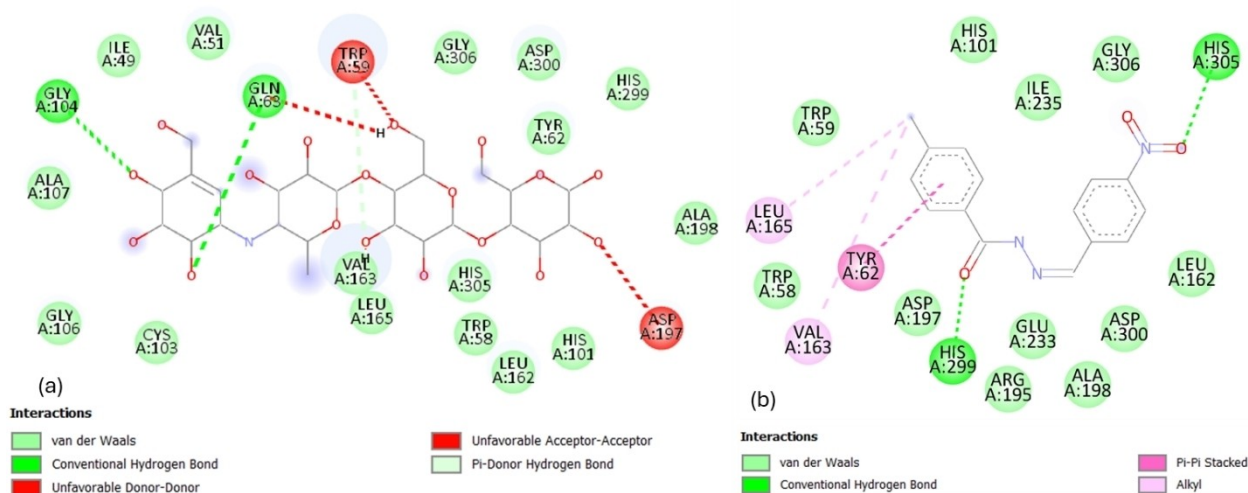


Figure 14. 2D diagram of the receptor-ligand interactions between porcine  $\alpha$ -amylase (PDB ID: 1OSE) and (a) acarbose and (b) BB4.

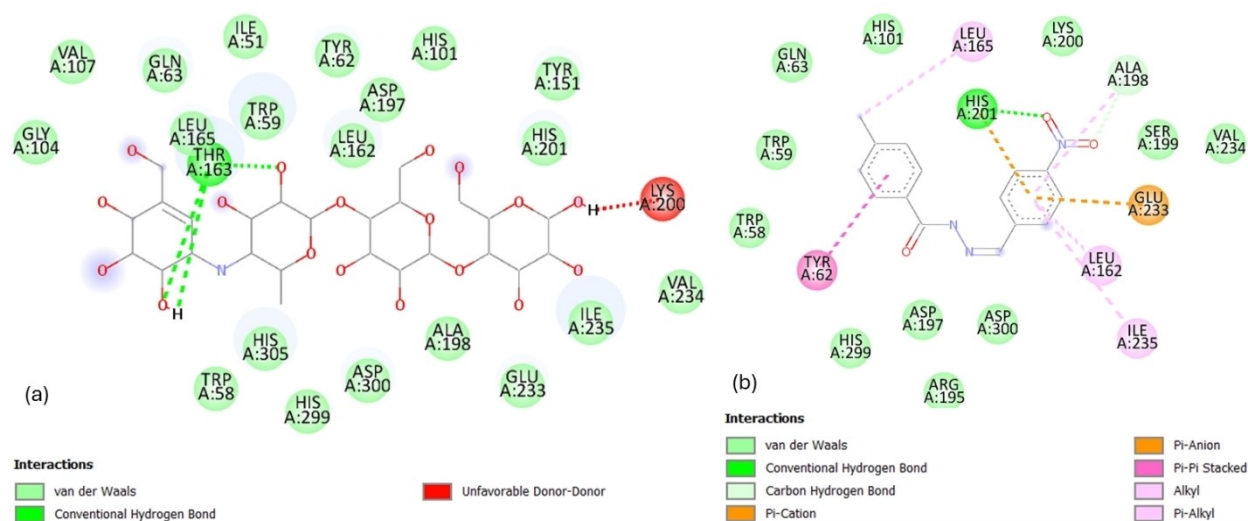


Figure 15. 2D diagram of the receptor-ligand interactions between pancreatic  $\alpha$ -amylase (PDB ID: 2QV4) and (a) acarbose and (b) BB4.

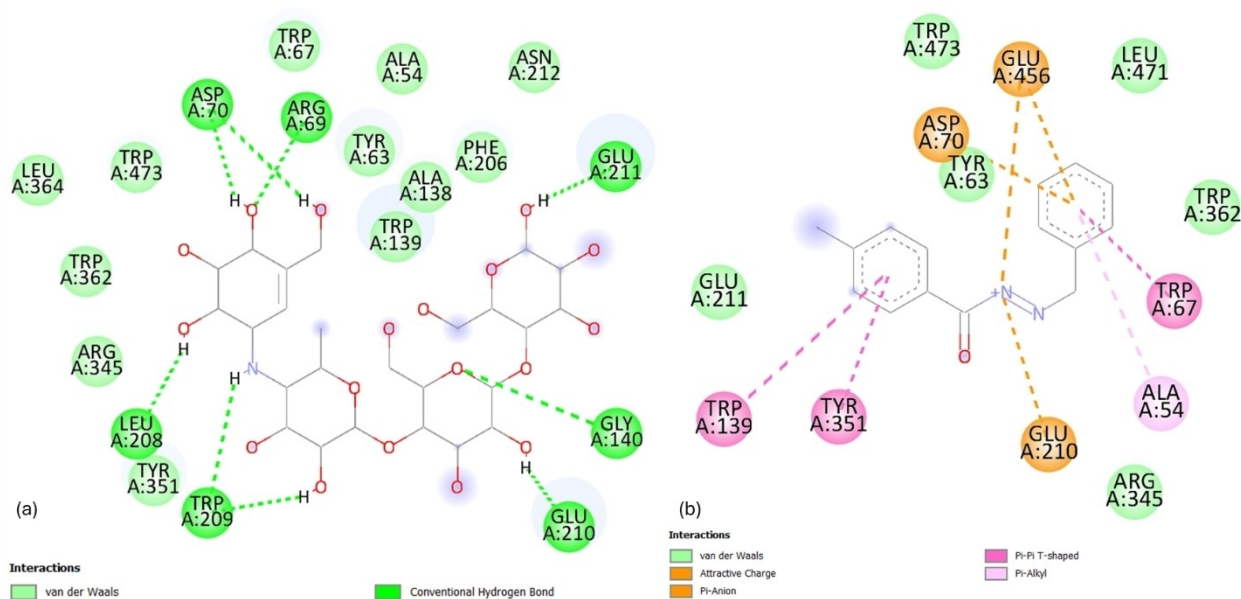


Figure 16. 2D diagram of the receptor-ligand interactions between glycoamylase (PDB ID: 2F6D) and (a) acarbose and (b) BB3.

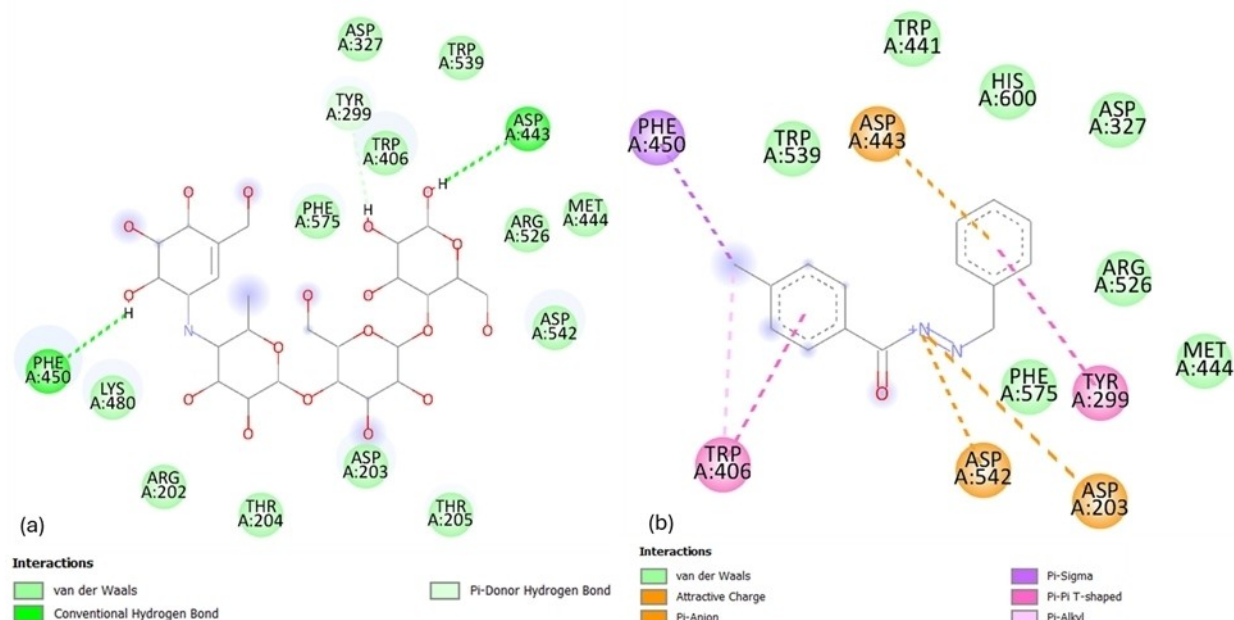
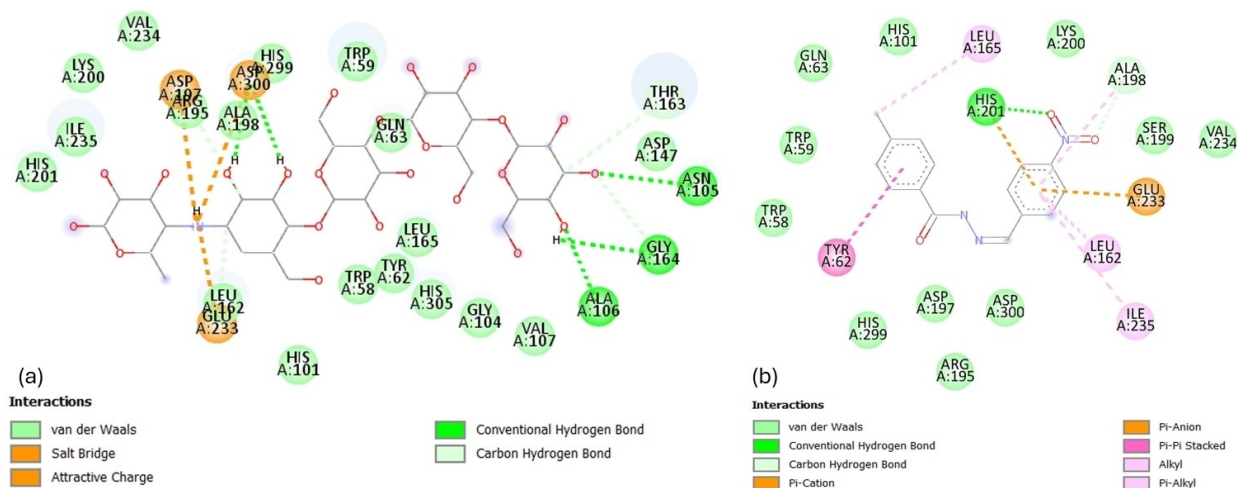


Figure 17. 2D diagram of the receptor-ligand interactions between human maltase-glycoamylase (PDB ID: 2QMJ) and (a) acarbose and (b) BB3.

different kind of interactions. Some of the interactions found in the co-crystallized ligand-2QV4 complex include salt bridge attractive charge with Asp197, Asp300 and Glu233. Conventional hydrogen bond with Asn105, Ala106 and Gly164; and carbon hydrogen bonds interaction with Thr163, Trp59 and Ile235. The 2QV4-BB4 complex is stabilized by a conventional hydrogen bond interaction with His201 residue, carbon hydrogen bond interaction Ala198, dual (pi-cation and pi-anion) interactions with Glu233. Also, pi-pi stacked interaction with Tyr62, alky and pi-alkyl interactions with Leu165, Leu162 and Ile235 amino acid residues.

For glucoamylase protein (PDB ID: 2QMJ), the binding energies of its co-crystallized ligand and BB3 ligand when docked unto the protein are  $-7.7$  and  $-7.5$ , respectively. These suggest that the top performing BB3 ligand has inhibition potential as strong as that of the co-crystallized ligand of the protein. The interactions involved are presented in Figure 19. Notably, the co-crystallized ligand has salt bridge and attractive charge interactions with Asp443, Asp542 and Asp203 residues. Conventional hydrogen bond with His600, Asn207 and Arg526 residues; and carbon hydrogen bond with Thr205, Trp406 and Tyr299 residues. The 2QMJ-BB3 complex is stabilized by



**Figure 18.** 2D diagram of the receptor-ligand interactions between pancreatic  $\alpha$ -amylase (PDB ID: 2QV4) and (a) co-crystallized (acarbose) and (b) **BB4**.

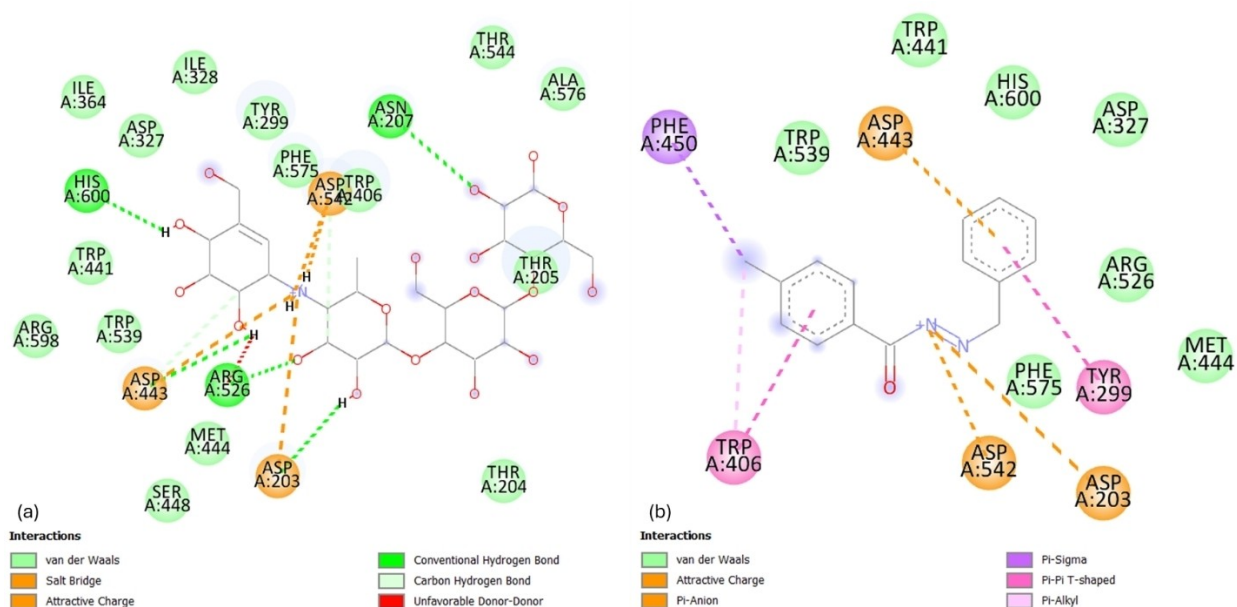


**Figure 19.** 2D diagram of the receptor-ligand interactions between pancreatic  $\alpha$ -amylase (PDB ID: 2QMJ) and (a) co-crystallized (acarbose) ligand and (b) **BB3**.

attractive charge and pi-anion interactions with Asp443, Asp542 and Asp203 residues; pi-pi T-shaped interaction with Tyr299 and Trp406; and a pi-sigma interaction with Phe450 amino acid residue. Other interactions include pi-alkyl and van der Waals interactions.

### 3. Conclusions

In summary, this study focused on the principles of using a bioactive molecule with multiple targets to discover lead compounds. We synthesized and characterized hydrazone Schiff base derivatives (**BB1**–**BB6**) using standard physicochemical and analytical techniques to confirm their structures. Crystal structures of **BB2**, **BB4**, and **BB6** were also reported. The compounds were then evaluated for their pharmacological

activities, specifically in terms of antioxidant and antidiabetic effects. In vitro techniques were employed to assess their performance in various assays, including DPPH, FRAP, NO radical scavenging,  $\alpha$ -glucosidase inhibition, and  $\alpha$ -amylase inhibition.

The results indicated that the compounds demonstrated multi-activity and exhibited potency in the DPPH and  $\alpha$ -glucosidase assays. Among the tested compounds, **BB4** showed the highest efficacy, followed by **BB2**, **BB5**, **BB6**, **BB3**, and **BB1**. Furthermore, a computational study was conducted on all the compounds. The chemical reactivity indices, such as quantum chemical parameters, frontier molecular orbital maps, and molecular electrostatic potential maps, provided insights into the chemical reactivity of the Schiff bases. They supported the fact that **BB2** and **BB4** are the most chemically reactive. As initially anticipated, the enhanced activity of these two

compounds can be attributed to the presence of the electron-withdrawing group, NO<sub>2</sub>, which deactivates certain positions in the ring and makes them susceptible to electrophilic aromatic substitution.

The molecular docking simulation revealed that **BB4** has the strongest inhibition capacity against  $\alpha$ -amylase protein, while **BB3** has the strongest inhibition capacity against  $\alpha$ -glucosidase protein.

## Supplementary Materials Summary

Supplementary crystallographic data for the compounds mentioned in the article can be obtained from the Cambridge Crystallographic Data Centre (CCDC) free of charge. The CCDC numbers for the supplementary crystallographic data are as follows: CCDC no: 2325385 (**BB2**), CCDC no: 232586 (**BB4**), and CCDC no: 232587 (**BB6**).

To access the supplementary crystallographic data, please visit the Cambridge Crystallographic Data Centre's website at [http://www.ccdc.cam.ac.uk/data\\_request/cif](http://www.ccdc.cam.ac.uk/data_request/cif).

Additionally, other supporting information associated with the article can be found in the online version at <https://doi.org/10.1002/slct.202401631>.

## Declaration of Competing Interest

The authors declare that they have no conflicts of interest regarding this study.

## Author Contributions

All authors contributed to the conception and design of the study, acquisition of data, analysis, and interpretation of results. They were all involved in drafting the manuscript and revising it critically for important intellectual content. All authors have given final approval of the version to be published.

## Acknowledgements

Dr. I. Waziri and Dr. T. L. Yusuf would like to express their gratitude to the URC for awarding the Postdoctoral Research Fellowship (PDRF). The authors also extend their thanks to the South African National Research Foundation (NRF) for providing funding support through Grant No. 111706 to cover running expenses, and center for synthesis and catalysis of the department of chemical science, university of Johannesburg. Furthermore, the authors acknowledge the Center for High Performance Computing (CHPC) in South Africa for generously providing the computational resources necessary for this research project.

## Conflict of Interests

The authors declare no conflict of interest.

## Data Availability Statement

The data that support the findings of this study are available in the supplementary material of this article.

**Keywords:** Free radicals · Oxidative stress · Diabetics · Schiff bases · Hydrazones

- [1] H. R. Afzal, N. u. H. Khan, K. Sultana, A. Mobashar, A. Lareb, A. Khan, A. Gull, H. Afzaal, M. T. Khan, M. Rizwan, *ACS Omega* **2021**, *6*, 4470.
- [2] H. Shirinzadeh, M. Ghaliya, A. Tascioglu, F. I. Adjali, G. Gunesacar, H. Gurer-Orhan, S. Suzen, *Brazilian Journal of Pharma. Sci.* **2020**, *56*, e18124.
- [3] G. Pizzino, N. Irrera, M. Cucinotta, G. Pallio, F. Mannino, V. Arcoraci, F. Squadrito, D. Altavilla, A. Bitto, *Oxidative medicine and cellular longevity* **2017**, *2017*(1), 8416763.
- [4] H. Shirinzadeh, E. Neuhaus, E. I. Erguc, A. T. Aliyev, H. Gurer-Orhan, S. Suzen, *Bioorg. Chem.* **2020**, *104*, 104219.
- [5] J. A. Berliner, J. W. Heinecke, *Free Radical Biol. Med.* **1996**, *20*, 707.
- [6] C. K. Glass, K. Saijo, B. Winner, M. C. Marchetto, F. H. Gage, *Cell* **2010**, *140*, 918.
- [7] S. I. Grivennikov, F. R. Greten, M. Karin, *Cell* **2010**, *140*, 883.
- [8] C. Nathan, A. Ding, *Cell* **2010**, *140*, 871.
- [9] M. Brewer, *Compr. Rev. Food Sci. Food Saf.* **2011**, *10*, 221.
- [10] H. Sies, *Exp. Physiol.: Trans. Integr.* **1997**, *82*, 291.
- [11] S. Suzen, B. Tekiner-Gulbas, H. Shirinzadeh, D. Uslu, H. Gurer-Orhan, M. Gumustas, S. A. Ozkan, *J. Enzyme Inhib. Med. Chem.* **2013**, *28*, 1143.
- [12] M. F. Nagoor Meeran, S. N. Goyal, K. Suchal, C. Sharma, C. R. Patil, S. K. Ojha, *Front. Pharmacol.* **2018**, *9*, 892.
- [13] J. Park, H.-J. Jang, *MCT* **2017**, *13*, 1.
- [14] I. Waziri, M. T. Kelani, M. O. Oyedeji-Amusa, A. K. Oyebamiji, L.-C. C. Coetzee, A. S. Adeyinka, A. J. Muller, *J. Mol. Struct.* **2023**, *1276*, 134756.
- [15] I. Waziri, T. L. Yusuf, E. Akintemi, M. T. Kelani, A. Muller, *J. Mol. Struct.* **2023**, *1273*, 134382.
- [16] T. L. Yusuf, I. Waziri, K. A. Olofinisan, E. O. Akintemi, E. C. Hosten, A. J. Muller, *J. Mol. Liq.* **2023** 122845.
- [17] M. Bashir, A. A. Dar, I. Yousuf, *ACS Omega* **2023**, *8*, 3026.
- [18] B. Kumar, J. Devi, A. Dubey, A. Tufail, B. Taxak, *Sci. Rep.* **2023**, *13*, 15906.
- [19] A. Boora, J. Devi, K. Lal, T. Rom, A. K. Paul, *Inorg. Chim. Acta* **2024**, *564*, 121940.
- [20] P. G. Avaji, C. V. Kumar, S. A. Patil, K. Shivananda, C. Nagaraju, *Eur. J. Med. Chem.* **2009**, *44*, 3552.
- [21] L. M. Lima, F. S. Frattani, J. L. Dos Santos, H. C. Castro, C. A. M. Fraga, R. B. Zingali, E. J. Barreiro, *Eur. J. Med. Chem.* **2008**, *43*, 348.
- [22] B. Taxak, J. Devi, A. Dubey, B. Kumar, A. Tufail, S. Pachwania, A. Boora, *Appl. Organomet. Chem.* **2024**, *38*, e7323.
- [23] A. Zengin, K. Serbest, M. Emirik, M. Özil, E. Menteşe, Ö. Faiz, *J. Mol. Struct.* **2023**, *1278*, 134926.
- [24] J. Devi, S. Pachwania, *Phosphorus Sulfur Silicon Relat. Elem.* **2021**, *196*, 1049.
- [25] S. Omid, A. Kakanejadifard, *RSC Adv.* **2020**, *10*, 30186.
- [26] E. Moradinia, M. Mansournia, Z. Aramesh-Boroujeni, A. K. Bordbar, *Appl. Organomet. Chem.* **2019**, *33*, e4893.
- [27] J. J. Tree, D. Wang, C. McInally, A. Mahajan, A. Layton, I. Houghton, M. Elofsson, M. P. Stevens, D. L. Gally, A. J. Roe, *Infect. Immun.* **2009**, *77*, 4209.
- [28] M. C. Mandewale, B. Thorat, D. Shelke, R. Yamgar, *Bioinorg. Chem. Appl.* **2015**, *1*, 153015.
- [29] C. F. de Faria, T. Moreira, P. Lopes, H. Costa, J. R. Krewall, C. M. Barton, S. Santos, D. Goodwin, D. Machado, M. Viveiros, *Biomed. Pharmacother.* **2021**, *144*, 112362.
- [30] S. Khan, M. Tariq, M. Ashraf, S. Abdullah, M. Al-Rashida, M. Khalid, P. Taslimi, M. Fatima, R. Zafar, Z. Shafiq, *Bioorg. Chem.* **2020**, *102*, 104082.
- [31] Ö. Aslanhan, E. Kalay, F. S. Tokali, Z. Can, E. Şahin, *J. Mol. Struct.* **2023**, *1279*, 135037.

- [32] S. Ahmad, M. Khan, N. U. Rehman, M. Ikram, S. Rehman, M. Ali, J. Uddin, A. Khan, A. Alam, A. Al-Harrasi, *Molecules* **2022**, *27*, 6906.
- [33] R. R. Ezz Eldin, M. A. Saleh, M. H. Alotaibi, R. K. Alsuair, Y. A. Alzahrani, F. A. Alshehri, A. F. Mohamed, S. M. Hafez, A. A. Althoqapy, S. K. Khirala, *J. Enzyme Inhib. Med. Chem.* **2022**, *37*, 1098.
- [34] H. Khan, F. Jan, A. Shakoar, A. Khan, A. F. AlAsmari, F. Alasmari, S. Ullah, A. Al-Harrasi, M. Khan, S. Ali, *Sci. Rep.* **2024**, *14*, 11410.
- [35] G. Zarrinzadeh, M. Tajbaksh, R. Hosseinzadeh, Z. Ghanbarimasir, M. Roudbary, M. Mohseni, H. Nadri, *J. Mol. Struct.* **2023**, *1293*, 136284.
- [36] Z. Moussa, M. Al-Mamary, S. Al-Juhani, S. A. Ahmed, *Heliyon* **2020**, *6*, e05019.
- [37] P. Mohan, R. Usha, G. P. Kalaigan, V. Muralidharan, *J. Chem.* **2013**, *2013*, 541691.
- [38] I. Waziri, H. M. Masena, T. L. Yusuf, L.-C. C. Coetzee, A. S. Adeyinka, A. J. Muller, *New J. Chem.* **2023**, *47*, 17853.
- [39] G. M. Sheldrick, *Acta Crystallogr. Sect. A* **1990**, *46*, 467.
- [40] T. Schulz, K. Meindl, D. Leusser, D. Stern, J. Graf, C. Michaelsen, M. Ruf, G. M. Sheldrick, D. Stalke, *J. Appl. Crystallogr.* **2009**, *42*, 885.
- [41] G. Sheldrick, *Acta Crystallogr. Sect. A Found. Adv.* **2015**, *71*, 3.
- [42] G. Sheldrick, *Struct. Chem.* **2015**, *71*, 3.
- [43] C. F. Macrae, I. Sovago, S. J. Cottrell, P. T. Galek, P. McCabe, E. Pidcock, M. Platings, G. P. Shields, J. S. Stevens, M. Towler, *J. Appl. Crystallogr.* **2020**, *53*, 226.
- [44] C. F. Macrae, I. J. Bruno, J. A. Chisholm, P. R. Edgington, P. McCabe, E. Pidcock, L. Rodriguez-Monge, R. Taylor, J. Streek, P. A. Wood, *J. Appl. Crystallogr.* **2008**, *41*, 466.
- [45] A. Turkoglu, M. E. Duru, N. Mercan, I. Kivrak, K. Gezer, *Food Chem.* **2007**, *101*, 267.
- [46] G. C. Lakshmi, S. Ananda, N. M. M. Gowda, *Synth. React. Inorg. Met.-Org. Nano-Met. Chem.* **2011**, *41*, 413.
- [47] G. A. Kurian, S. Suryanarayanan, A. Raman, J. Padikkala, *Chin. Med.* **2010**, *5*, 1.
- [48] L. J. Shai, P. Masoko, M. P. Mokgotho, S. R. Magano, A. Mogale, N. Boaduo, J. N. Eloff, *S. Afr. J. Bot.* **2010**, *76*, 465.
- [49] M. Ahmadi, M. Jahed Motlagh, A. Rahmani, M. Zolfaghazadeh, P. Shariatpanahi, T. Chermack, L. Coons, J. Cotter, E. Eyiah-Donkor, V. Poti, *Macromolecules* **2005**, *24*, 1.
- [50] R. Dennington, T. A. Keith, J. M. Millam, Semichem Inc Shawnee Mission KS **2016**, *5*, 143.
- [51] L. Piela, *Ideas Quantum Chem* **2014**.
- [52] C. U. Ibeji, D. C. Akintayo, H. O. Oluwasola, E. O. Akintemi, O. G. Onwukwe, O. M. Eziomume, *Sci. Rep.* **2023**, *13*, 3265.
- [53] T. L. Yusuf, I. Waziri, K. A. Olofinson, E. O. Akintemi, E. C. Hosten, A. J. Muller, *J. Mol. Liq.* **2023**, *389*, 122845.
- [54] L. V. Van, E. C. Pham, C. V. Nguyen, N. T. N. Duong, T. V. Le Thi, T. N. Truong, *Biomed. Pharmacother.* **2022**, *146*, 112611.
- [55] T. L. Yusuf, E. O. Akintemi, S. Olagboye, G. F. Tolufashe, *Phys. Sci. Rev.* **2021**, *8*, 535.
- [56] S. Nakamura, K. Takahira, G. Tanabe, T. Morikawa, M. Sakano, K. Ninomiya, M. Yoshikawa, O. Muraoka, I. Nakanishi, *Bioorg. Med. Chem. Lett.* **2010**, *20*, 4420.
- [57] S. Dallakyan, A. J. Olson, *Chem. Biol.: Methods and Protocols* **2015** 243.
- [58] B. Y. G. Mountessou, A. W. Ngooune, A. S. W. Mbobda, E. O. Akintemi, H.-G. Stammer, S. F. Kouam, J. C. Tchouankeu, B. N. Lenta, N. Sewald, T. Singh, *J. Mol. Struct.* **2023**, 136003.
- [59] T. Arora, J. Devi, A. Dubey, A. Tufail, B. Kumar, *Appl. Organomet. Chem.* **2023**, *37*, e7209.
- [60] T. Hong, J.-Y. Yin, S.-P. Nie, M.-Y. Xie, *Food Chem. X* **2021**, *12*, 100168.
- [61] K. B. Beć, J. Grabska, C. W. Huck, *Anal. Chim. Acta* **2020**, *1133*, 150.
- [62] B. Taxak, J. Devi, S. Kumar, S. Asija, *Inorg. Chem. Commun.* **2023**, *158*, 111473.
- [63] A. Boora, J. Devi, T. Rom, A. K. Paul, *J. Mol. Struct.* **2023**, *1284*, 135386.
- [64] J. Coates, *Interpretation of Infrared Spectra, A Practical Approach*, **2000**, *15*, 10815.
- [65] R. A. Pratiwi, A. B. D. Nandiyanto, *Indonesian J. Educat. Res. Technol.* **2022**, *2*, 1–20.
- [66] R. J. Anderson, D. J. Bendell, P. W. Groundwater, *Org. Spectroscopic Analysis, Royal Soc. Chem.* **2004**, *22*, 182.
- [67] M. S. Lee, E. H. Kerns, *Mass Spectrom. Rev.* **1999**, *18*, 187.
- [68] M. Wenzel, A. Casini, *Coord. Chem. Rev.* **2017**, *352*, 432.
- [69] A. D. Fedichkina, D. S. Koshelev, A. A. Vashchenko, L. O. Tcelykh, A. S. Goloveshkin, V. E. Gontcharenko, E. V. Latipov, A. V. Medved'ko, S. Z. Vatsadze, A. S. Burlov, *J. Lumin.* **2022**, *244*, 118702.
- [70] N. Kausar, S. Murtaza, M. N. Arshad, R. S. Z. Saleem, A. M. Asiri, S. Kausar, A. A. Altaf, A. Tatheer, A. Y. Elnaggar, S. M. El-Bahy, *RSC Adv.* **2022**, *12*, 154.
- [71] P. Jeeva, D. Barathi, R. Mani, M. Louhi-Kultanen, G. Vinitha, A. G. Al-Sehemi, *J. Mol. Struct.* **2022**, *1254*, 132375.
- [72] R. Vona, L. Pallotta, M. Cappelletti, C. Severi, P. Matarrese, *Antioxidants (Basel)* **2021**, *10*, 201.
- [73] S. Baliyan, R. Mukherjee, A. Priyadarshini, A. Vibhuti, A. Gupta, R. P. Pandey, C.-M. Chang, *Molecules* **2022**, *27*, 1326.
- [74] M. Taha, N. H. Ismail, W. Jamil, S. Yousuf, F. M. Jaafar, M. I. Ali, S. M. Kashif, E. Hussain, *Molecules* **2013**, *18*, 10912.
- [75] I. G. Munteanu, C. Apetrei, *Int. J. Mol. Sci.* **2021**, *22*, 3380.
- [76] S. Aytac, O. Gundogdu, Z. Bingol, I. Gulcin, *Pharmaceutica* **2023**, *15*, 779.
- [77] S. B. Nimse, D. Pal, *RSC Adv.* **2015**, *5*, 27986.
- [78] U. Hossain, A. K. Das, S. Ghosh, P. C. Sil, *Food Chem. Toxicol.* **2020**, *145*, 111738.
- [79] W. U. Islam, A. Khan, F. Khan, S. Ullah, M. Waqas, H. Khan, M. Khan, S. M. Rahman, S. Ali, A. Mateen, *J. Biomol. Struct. Dyn.* **2024**, *9*, 1–12.
- [80] E. A. Yildiz, Y. Pepe, D. Erdener, A. Karatay, B. Boyacioglu, H. Ünver, G. Yapar, N. Demir, M. Yildiz, A. Elmali, *J. Mol. Struct.* **2023**, *1286*, 135611.
- [81] A. A. Haase, S. A. Markham, H. A. Murakami, J. Hagan, K. Kostenkova, J. T. Koehn, C. Uslan, C. N. Beuning, L. Brandenburg, J. M. Zdrozny, *New J. Chem.* **2024**, *48*, 12893.
- [82] M. Hoelm, J. Adamczyk, K. Wzgarda-Raj, M. Palusiak, *J. Org. Chem.* **2023**, *88*, 2132.
- [83] I. Waziri, M. T. Kelani, M. O. Oyedeji-Amusa, A. K. Oyebamiji, L.-C. C. Coetzee, A. J. Muller, *Heliyon* **2024**, *10*, e26632.
- [84] A. C. Gaudio, A. Korolkovas, Y. Takahata, *J. Pharm. Sci.* **1994**, *83*, 1110.
- [85] E. O. Akintemi, K. K. Govender, T. Singh, *Comput. Theor. Chem.* **2022**, *1210*, 113658.
- [86] V. Lokshin, M. Sigalov, N. Larina, V. Khodorkovsky, *RSC Adv.* **2021**, *11*, 934.
- [87] S. Irle, T. Krygowski, J. Niu, W. Schwarz, *J. Org. Chem.* **1995**, *60*, 6744.
- [88] T. E. Olalekan, E. O. Akintemi, B. Van Brecht, G. M. Watkins, *Bull. Chem. Soc. Ethiop.* **2023**, *37*, 675.
- [89] I. Alkorta, J. J. Perez, *Int. J. Quantum Chem.* **1996**, *57*, 123.
- [90] B. Y. G. Mountessou, A. S. W. Mbobda, H.-G. Stammer, E. O. Akintemi, M. B. Mbah, G. M. Happi, S. F. Kouam, B. N. Lenta, N. Sewald, T. Singh, *J. Mol. Struct.* **2023**, *1282*, 135185.
- [91] M. D. Olawale, E. O. Akintemi, N. D. Ojo, A. Y. Isaac, H. Su, J. A. Obaleye, *J. Comput. Biophys. Chem.* **2023**, *22*, 845.
- [92] S. Sasidharan, P. Saudagar, *Advances in Protein Molecular and Structural Biology/Methods*, Elsevier **2022**, *6*, 373.
- [93] M. Bachwani, R. Kumar, *IJRAP* **2011**, *2*, 1746.
- [94] S. Agarwal, R. Mehrotra, *JSM Chem.* **2016**, *4*, 1024.

Manuscript received: April 5, 2024